NACA

RESEARCH MEMORANDUM

PRELIMINARY INVESTIGATION OF A SUBMERGED INLET AND A NOSE INLET IN THE TRANSONIC FLIGHT RANGE WITH FREE-FALL MODELS

By James Selna

Ames Aeronautical Laboratory
Moffett Field, Calif.

NATIONAL ADVISORY COMMITTEE
FOR AERONAUTICS

WASHINGTON
June 18, 1951

NATIONAL ADVISORY COMMITTEE FOR AERONAUTICS

RESEARCH MEMORANDUM

PRELIMINARY INVESTIGATION OF A SUBMERGED INLET AND A NOSE INLET IN THE TRANSONIC FLIGHT RANGE WITH FREE-FALL MODELS

By James Selna

SUMMARY

An NACA submerged inlet and an NACA series I nose inlet were installed in bodies of 12.4 fineness ratio to determine the drag and pressure-recovery characteristics of each body-inlet configuration. The tests were conducted, with large-scale free-fall models released at an altitude of 40,000 feet, for mass-flow ratios of about 0.4 and 0.7 over a Mach number range of about 0.70 to 1.10.

The results show that neither inlet had any significant effect on the Mach number of drag divergence. The external drag of the submerged inlet model was indicated to be larger than that of the nose-inlet model at a mass flow ratio of 0.7. The difference in drag between the two inlet models when expressed in terms of the drag coefficient for an assumed airplane (with a ratio of frontal fuselage area to wing area of 0.06) would amount to about 0.0006 at subsonic speeds preceeding drag divergence and about 0.0012 at supersonic speeds.

The ram-recovery ratios for the submerged-inlet model were in general agreement with those obtained in previous subsonic researches. Above a Mach number of 1, the pressure recovery decreased gradually.

INTRODUCTION

In order to provide space in the nose of an aircraft fuselage for housing radar and armament, attention has been given to the location of air inlets on the sides of the fuselage. A side inlet which has shown promise is the NACA submerged inlet which was developed in wind-tunnel tests reported in references 1 and 2. Additional wind-tunnel tests of this inlet have been carried out at subsonic speeds as reported in references 3 to 10. Small-scale tests of the NACA submerged inlet in the low transonic range (up to a Mach number of 0.94) are reported in reference 11. Other tests in the transonic range have been conducted up

to a local Mach number of 1.14 using the tunnel bump technique (reference 12) and in flight up to a local Mach number of 1.08 using the NACA wing-flow method (reference 13). The bulk of these tests were concerned with pressure-recovery and pressure-distribution characteristics of the NACA submerged inlet. Drag data on these inlets at subsonic speeds are limited (references 2 and 7), while at transonic speeds drag information is not available.

The purpose of the present investigation was to evaluate the drag and pressure recovery of a submerged-inlet and a nose-inlet model at relatively large Reynolds numbers to compare the drag of the two inlet models. The investigation was conducted by utilizing a free-fall recoverable model which permits tests at relatively large scale in the transonic range. This technique permits the use of standard instruments and the recovery of the model and instruments intact.

The current report provides data for mass-flow ratios of about 0.4 and 0.7 through a Mach number range of approximately 0.70 to 1.10.

The tests were conducted in the desert regions of Edwards Air Force Base at Muroc, California.

SYMBOLS

a	speed of sound, feet per second
A	cross-sectional area of one duct, square feet
a_x	horizontal acceleration of model, feet per second, second
a_y	vertical acceleration of model, feet per second, second
c_p	specific heat at constant pressure, Btu per pound, $^{\circ}F$
c_v	specific heat at constant volume, Btu per pound, $^{\circ}F$
C_{D_T}	total drag coefficient $\left(C_{D_T} = \frac{D_T}{q_o S}\right)$, dimensionless
C_{D_E}	external drag coefficient $\left(C_{D_E} = C_{D_T} - C_{D_I}\right)$, dimensionless
C_{D_I}	internal drag coefficient $\left(\frac{D_I}{q_o S}\right)$, dimensionless

[redacted]

D_T	total drag, pounds
D_E	external drag $\left(D_T-D_I\right)$, pounds
D_I	internal drag, pounds
g	acceleration due to gravity, 32.16 feet per second, second
h	pressure altitude in a standard atmosphere, feet
H	total pressure, pounds per square foot
$\frac{H-p_o}{H_o-p_o}$	ram-recovery ratio, dimensionless
J	mechanical equivalent of heat, 778 foot-pounds per Btu
L	vertical distance below release altitude, feet
M	Mach number, dimensionless
m	mass flow, slugs per second
$\frac{m_1}{m_o}$	mass-flow ratio $\left(\frac{\rho_1 A_1 V_1}{\rho_o A_1 V_o}\right)$, dimensionless
p	static pressure, pounds per square foot
q	dynamic pressure $\left(\frac{1}{2}\rho V^2\right)$, pounds per square foot
q_c	impact pressure $(H-p)$, pounds per square foot
S	cross-sectional area of model at maximum diameter, square feet
T	temperature, ^oF absolute
t	time after release of model, seconds
V	true airspeed (aM), feet per second
V_x	horizontal component of model axial velocity relative to air, feet per second

[redacted]

V_y	vertical component of model axial velocity relative to air, feet per second
V_w	horizontal component of wind velocity in a vertical plane tangent to the flight path (positive direction opposite to V_x), feet per second
W	weight of model, pounds
γ	ratio of specific heats $\left(\frac{c_p}{c_v}\right)$, dimensionless
φ	angle between model axis and horizontal plane, degrees
ρ	mass density of air, slugs per cubic foot
η	compressibility factor $\left(\frac{M^2}{4} + \frac{M^4}{16} + \frac{M^6}{1600} \cdots\right)$
R,K,B	constants

Subscripts

i	measured value at airspeed head or temperature probe
o	free stream
e	station where the air discharged from the model has returned to free-stream static pressure
86.5, 97, 134	model stations, inches
a,b,c,d	separate measurements made at a given model station
1	duct entrance (station 62 for submerged inlet, station 1 for nose inlet)
s	surface

TECHNIQUE AND MODELS

The present investigation was conducted by utilizing the free-fall recoverable-model technique. In this technique, the model is recovered by parachute after first being decelerated to a safe parachute-launching speed by the extension of an umbrella-type dive brake, shown on a model without inlets in figure 1. The portion of the fuselage aft of the dive brake houses the parachute. Test data are recorded by standard NACA flight instruments contained in the main portion of the fuselage.

The model is released from a carrier airplane at approximately 40,000 feet. A photograph of one model upon release from the airplane is shown in figure 2. The model falls freely until it attains a Mach number of about 1.1 at about 18,000 feet where the recovery process is initiated. The dive brake slows the model down to a speed of approximately 250 miles per hour. At this speed, the parachute is released and the model is lowered to the ground at a speed of less than 50 feet per second which permits recovery of the model and instruments. The damage to the model is negligible if the model nose boom is successfully embedded in the ground as shown in figure 3.

The model without inlets (hereinafter referred to as the basic model) used for the tests of this report is shown in figures 1, 2, 3, and 4. The model length, exclusive of airspeed boom, was 211 inches and the maximum diameter was 17 inches giving a fineness ratio of 12.4. The weight of each model was about 1100 pounds. The fins on all models were at 0° incidence.

All external screws were flush with the skin and the hangers attaching the model to the airplane were retracted into the model after its release.

The details of the airspeed head used on all models are shown in figure 5.

The installation of NACA submerged inlets, ducting, and air exits is shown in figures 6 and 7. The submerged inlet was made up of a 7° ramp with curved diverging walls (see reference 2). Each duct had an inlet area of 13.62 square inches and an aspect ratio of 4. The necessity of discharging the air forward of the dive-brake region resulted in the outlet design shown.

The NACA series I nose-inlet model is shown in figures 8 and 9. The area of the annular inlet of this model was the same as that of the two submerged air entrances. The inlet was, in the notation of reference 14, an NACA series I-35.8-600 nose inlet with a 1.5-inch-diameter

[redacted]

nose boom (on which the airspeed head, fig. 5, was mounted) extending through the center of the inlet. The model aft of station 102 was identical with the submerged-inlet model.

In order to make the nose-inlet model comparable to the submerged-inlet model on a drag basis, an attempt was made to provide the same amount of usable volume in both models. Since the nose-inlet model was the same length as the submerged-inlet model, it had a greater volume and surface area than the submerged-inlet model. The nose-inlet model, however, was considered suitable for comparison on a drag basis with the submerged-inlet model because the additional volume is almost entirely consumed by the additional ducting required for the nose inlet.

INSTRUMENTATION

The locations of the pressure tubes in the submerged-inlet model are shown in figure 6. Aft of the inlet, the pressure tubes provided in the nose-inlet model (fig. 8) were identical with those in the submerged-inlet model. Pressure rakes were installed in both ducts for flow symmetry; however, only those in the left duct were used in the current tests. A rake consisting of four total-pressure tubes was installed in the ducting at station 86.5 for the determination of pressure recovery and mass-flow ratio. A sonic throat was located in the ducting at station 97 for control and measurement of the flow rate through the ducting. Each inlet model was tested at mass-flow ratios of approximately 0.4 and 0.7 by using sonic throats of about 50 and 80 percent of the duct-inlet area. The static pressure at the throat (station 97) and the pressure drop from station 86.5 to station 97 were measured to check the presence of sonic flow in the throat. A rake consisting of four total-pressure probes and four static-pressure probes was inserted in the ducting at station 134 for the determination of the internal drag. Orifices (fig. 6) were installed along the ramp center lines to determine the ramp-pressure distribution. For one test drop of a nose-inlet model, a total-pressure rake was installed at the inlet as shown in figure 8(b). The data were all recorded on standard NACA recording instruments, which were compensated for temperature effects throughout the temperature range experienced within the heated interior of the models. The model instruments and their functions, ranges, and estimated accuracies based on laboratory calibrations are listed in table I.

The pressure-measuring system was designed to render negligible any effects of lag. For the longer lines, such as the airspeed lines, the tubing was 3/16-inch inside diameter. Shorter tubes were 1/8-inch inside diameter.

[redacted]

Instruments were installed in a heated compartment of the carrier airplane to record atmospheric data during the ascent of the carrier airplane. The instruments used, their purpose, and the estimated accuracy of these instruments, based on laboratory calibrations, are given in table II.

TESTS

Prior to the dropping of each model, the atmosphere through which the model was to fall was surveyed. This was accomplished by the instruments in the carrier airplane which were operated at about 1,000-foot intervals during the ascent to 40,000 feet.

After attaining a release altitude of approximately 40,000 feet, the airplane was oriented for the drop run. Every effort was made to maintain level flight during this run. The airplane instruments were put in operation for a period of at least 10 seconds prior to release. This action also actuated the model instruments and assured that the instrument motors would be up to speed at the time of release.

After release, each model accelerated to a Mach number of about 1.1 as the instruments continuously recorded the data listed under instrumentation.

RESULTS

The methods employed for the evaluation of the free-stream Mach number, the mass-flow ratio, and the internal drag are described in the appendix.

A typical variation of the free-stream Mach number with time after release and of the model Reynolds number with Mach number is presented in figure 10.

The static-pressure-error coefficients for the airspeed head, evaluated from equations (1) to (11) of the appendix are presented in figure 11. The faired curves of figure 11 were employed as the values of the static pressure errors of the airspeed head. The total pressures in the ducts, particularly the total-pressure measurements at station 86.5 during the tests of the nose-inlet model, fluctuated with time. These fluctuations are believed to be the result of slight model oscillations during the free fall which caused changes in the amount of boundary-layer air flowing into each duct. In the case of the nose-inlet model tested at a mass-flow ratio of about 0.7, the measurements made near the inlet at station 1 (shown in fig. 12) indicate that the fluctuations are traceable to the boundary-layer air flowing along the

nose boom. These total-pressure fluctuations were insufficient to affect the drag results. However, a faired average of the total-pressure measurements at station 86.5 was used in evaluating the pressure recovery.

Although no measurements were made at station 1 during the tests of the nose-inlet model at a mass-flow ratio of about 0.4, the boundary-layer air flowing along the boom probably separated at a Mach number of about 1.07. Above this Mach number, the recorded accelerometer and duct pressure data showed large fluctuations. Consequently, the data beyond a Mach number of 1.07 for the test of the nose-inlet model at a mass-flow ratio of about 0.4 were of no value.

The mass-flow-ratio variation with Mach number at nominal mass-flow ratios of 0.4 and 0.7 are presented for both inlet models in figure 13. Figure 14 illustrates the internal drag-coefficient variation with Mach number for the submerged-inlet model and the nose-inlet model. These values were calculated only for use in determining the external drags of the models.

The variation of external drag coefficients of the basic model with Mach number is presented in figure 15. The total and external drag coefficients of the submerged-inlet model and the nose-inlet model are shown in figures 16 and 17. The drag data obtained at a mass flow ratio of 0.4 were known to be erroneous and are not presented. The external drags of the models are summarized in figure 18.

The ram-recovery ratios at station 86.5 and at the duct entrances (evaluated from duct efficiency factors) are given in figures 19 and 20, respectively, for the tests of the submerged-inlet model and the nose-inlet model. The ram-recovery ratios at the entrance of the nose-inlet model at a mass-flow ratio of about 0.7 were also estimated for several Mach numbers from the pressure measurements made at station 1 (fig. 12) and these data points are also included in figure 20(b). The pressure recoveries were averaged over the entrance area for the determination of the average pressure recovery from the limited data of figure 12.

The pressure distribution along the ramp of the submerged-inlet model at mass-flow ratios of about 0.4 and 0.7 for various Mach numbers are given in figure 21. The Mach number distributions along the ramp, based on the measured ramp pressures and free-stream total pressure, are presented in figure 22.

[redacted]

ACCURACY OF RESULTS

Based on the scatter of the experimental data of these tests and data from other similar free fall tests, the maximum errors involved in the evaluation of free-stream Mach number, mass-flow ratio, and external drag are tabulated below:

Quantity	Estimated maximum error
M_o	0.02 at a Mach number of 0.75
	0.01 at Mach numbers above 0.85
$\frac{m_1}{m_o}$	0.01
C_{D_E}	0.01 below a Mach number of 1
	0.005 above a Mach number of 1

The probable errors are less than these maximum values.

DISCUSSION OF RESULTS

Drag

The variations of internal drag coefficient with Mach number for the two mass-flow ratios are shown in figure 14. The internal drag coefficients increased with a decrease in mass-flow ratio. This is a result of the increased shock losses resulting from higher supersonic speeds in the nozzle aft of the sonic throat.

The external drag of the submerged inlet model is indicated to be greater than that of the nose inlet model throughout the test range at a mass flow ratio of 0.7. The difference between the external drag coefficients of the two models is negligible at a Mach number of 0.7 gradually increasing to about 0.01 at the subsonic Mach numbers preceeding drag divergence. At supersonic speeds, this difference in external drag coefficient is about 0.02. For a typical operational aircraft with a fuselage frontal area to wing area of about 0.06, this would amount to a change in airplane drag coefficient (based on wing area) of about 0.0006 at the subsonic Mach numbers preceeding drag divergence and about 0.0012 at supersonic speeds.

The results presented in figure 18 indicate that the drag of the nose-inlet model increased slightly with increasing mass-flow ratio at

[redacted]

Mach numbers greater than 0.8. Previous results at transonic speeds for a nose-inlet model (reference 15) have indicated the external drag to be essentially constant over a mass-flow ratio range of 0.4 to 0.8.

The outlet employed in the present tests was not of a conventional design, consequently there is little significance to a comparison of the external drag coefficients of the inlet models with that of the basic model. Since the same air-outlet configuration was employed for both inlet models, a comparison of the external drag coefficients for these models is justified.

Ram-Recovery Ratios

The ram-recovery ratios at station 86.5 and at the entrance are presented in figure 19 for the submerged-inlet model. The ram-recovery ratios, at both mass-flow ratios, increase gradually up to a free-stream Mach number of about 1, after which there is a slight decrease up to the maximum test Mach numbers.

The decreases in pressure recovery at Mach numbers above 1 are believed to be associated with shock losses along the inlet ramp. These decreases in pressure recovery are approximately equal to the losses associated with a normal shock at the maximum local ramp Mach numbers of figure 22. If the flow along the ramp does not separate at Mach numbers higher than those of the present tests, the pressure recovery will probably decrease gradually, as the shock losses increase, with increasing Mach number.

The ram recoveries obtained in the present investigation (fig. 19(b)) are in general agreement with those obtained in previous researches. The data obtained in reference 9 at a mass-flow ratio of 0.7 at about the same number of duct-entrance depths aft of the model nose are also shown in figure 19(b), and are in good agreement with the present results.

The ram-recovery ratios obtained for the nose-inlet model (fig. 20) are not particularly significant because they include the losses incurred in the boundary layer of the airspeed boom. As is well known, the ram recovery for the nose inlet, with the boom removed, would be essentially unity for the test Mach number range.

[redacted]

CONCLUDING REMARKS

An NACA submerged inlet and an NACA series I nose inlet were installed in bodies of 12.4 fineness ratio to determine the drag and pressure-recovery characteristics of each body-inlet configuration in the transonic range. The results show that neither inlet had any significant effect on the Mach number of drag divergence. The external drag of the submerged-inlet model was indicated to be larger than that of the nose inlet model at a mass-flow ratio of 0.7. The difference in drag coefficient (based on maximum body cross-sectional area) between the two inlet models was about 0.01 at the subsonic Mach numbers preceeding drag divergence and about 0.02 at the supersonic test Mach numbers. This difference in terms of the drag coefficient for an assumed airplane (with a ratio of frontal fuselage area to wing area of 0.06) would amount to about 0.0006 at subsonic speeds preceeding drag divergence and about 0.0012 at supersonic speeds.

The ram-recovery ratios measured for the submerged-inlet model were of the order of those obtained in previous investigations. The pressure recovery decreased slightly above a Mach number of 1. This decrease is attributed to increasing shock losses in the flow along the inlet ramp with increasing supersonic free-stream Mach numbers.

Ames Aeronautical Laboratory,
National Advisory Committee for Aeronautics,
Moffett Field, Calif.

[redacted]

APPENDIX

Method of Analysis of Data

The quantities desired include mass-flow ratio and internal drag as functions of free-stream Mach number.

The airspeed-head static pressure which is recorded in the model is in error due to the proximity of the static-pressure holes to the airspeed head and the model; therefore, before proceeding to evaluate the Mach number, it is necessary to establish the free-stream static pressure p_o as a function of time after release of the model.

Free-Stream Static Pressure

The free-stream static pressure was correlated with time after release of the model by (1) determining the vertical distance L the model fell from the release altitude as a function of time t by a step-by-step integration of the model acceleration, and (2) determining the free-stream static pressure p_o as a function of the vertical distance L, utilizing the atmospheric survey data obtained during ascent of the carrier airplane.

The vertical distance that the model fell as a function of time was evaluated from a step-by-step integration of the acceleration of the model. The method employed is valid only at zero lift and is similar to that given in reference 16.

Consider any time t, during the model free fall, at which the quantities L, V_x, V_y, φ, and D_T/W are known, where

$$\tan \varphi = \frac{V_y}{V_x} \tag{1}$$

and D_T/W (ratio of axial force to model weight) is continuously recorded as a function of time by the longitudinal accelerometer.

The problem is to determine the same quantities at a time $t + \Delta t$ and to repeat the process until L is known as a function of time throughout the model free fall. The vertical distance that the model falls in a time increment Δt is approximated as the product of the average velocity during the time increment and the time increment.

[redacted]

$$\Delta L = \left[\left(V_y \right)_t + \frac{\Delta V_y}{2} \right] \Delta t \tag{2}$$

where

$$\Delta V_y \equiv (a_y)_{t+\frac{1}{2}\Delta t} \, \Delta t \tag{3}$$

in which $(a_y)_{t+\frac{1}{2}\Delta t}$ is the average acceleration during the time increment, herein taken as the acceleration at a time $t+\frac{1}{2}\Delta t$. This acceleration was evaluated from the relationship

$$(a_y)_{t+\frac{1}{2}\Delta t} = g \left[1 - \left(\frac{D_T}{W} \right)_{t+\frac{1}{2}\Delta t} \sin (\varphi)_{t+\frac{1}{2}\Delta t} \right] \tag{4}$$

where the value of $(D_T/W)_{t+\frac{1}{2}\Delta t}$ is the value measured by the longitudinal accelerometer at a time $t+\frac{1}{2}\Delta t$. The angle employed in equation (4) is taken as a linear extrapolation of φ in the body of the step-by-step solution, or

$$(\varphi)_{t+\frac{1}{2}\Delta t} = \frac{3(\varphi)_t - (\varphi)_{t-\Delta t}}{2} \tag{5}$$

At the start of the computation (upon release from the airplane in level flight), $(\varphi)_{t-\Delta t}$ is not known and $(\varphi)_t$ is used in equation (4) for $(\varphi)_{t+\frac{1}{2}\Delta t}$.

In order to evaluate φ at the end of the time increment from equation (1), V_x at the end of the time increment must be determined. This is accomplished by determining V_x in a manner similar to the evaluation of V_y. That is,

$$\Delta V_x = (a_x)_{t+\frac{1}{2}\Delta t} \, \Delta t + \Delta V_w \tag{6}$$

where

$$(a_x)_{t+\frac{1}{2}\Delta t} = g \left[\left(\frac{D_T}{W} \right)_{t+\frac{1}{2}\Delta t} \cos (\varphi)_{t+\frac{1}{2}\Delta t} \right] \tag{7}$$

[redacted]

Thus, equation (2) can be integrated step by step to give L as a function of time.

For the next step (the determination of the free-stream static pressure as a function of L), the method employed was based on the fact that the difference in pressure between two geometric altitudes ΔL is a measure of the weight of fluid per unit area Δp_o between the two geometric levels. Thus,

$$g(\rho_o)_{av} \Delta L = \Delta p_o \tag{8}$$

where the subscript av refers to the average value over a vertical distance ΔL. Introducing pressure and temperature into equation (8) instead of ρ provides the expression

$$\Delta L = R \frac{(T_o)_{av}}{(p_o)_{av}} \Delta p_o \tag{9}$$

where R is the gas constant. Dividing equation (9) by the analogous equation for a standard atmosphere yields

$$\frac{\Delta L}{\Delta h} = \frac{(T_o)_{av}}{\left[(T_o)_{av}\right]_{\text{standard atmosphere}}} \tag{10}$$

where Δh is the pressure altitude increment in a standard atmosphere corresponding to a pressure increment Δp_o. The temperature used in equation (10) is free-stream static temperature T_o which is evaluated from the measured temperature T_1 and the effects of aerodynamic heating as follows:

$$T_o = T_1 - \frac{KV_o^2}{2gJc_p} = \frac{T_1}{1 + \frac{K}{5} M_o^2} \tag{11}$$

where K is a temperature recovery factor (reference 17). For the temperature probe employed, K was established as 0.76 in flight calibrations. Using equations (2) and (10) p_o is obtained as a function of L. Once p_o is established, the free-stream Mach number, a function of p_o/H_o, can be calculated. Also, the static-pressure error

[redacted]

of the airspeed head can be expressed in the usual form $\frac{p_1-p_o}{(q_c)_1}$ as a function of M_o.

Mass-Flow Ratio

Once the Mach number was established, the mass-flow ratio was evaluated from the values of the free-stream Mach number and the total pressures determined at station 86.5 by the relationship

$$\frac{m_1}{m_o} = \frac{B}{M_o} \frac{(H)_{86.5}}{H_o} \frac{(A)_{87}}{A_1} \left(\frac{2}{\gamma+1} + \frac{\gamma-1}{\gamma+1} M_o^2 \right)^{\frac{\gamma+1}{2(\gamma-1)}} \tag{12}$$

which is identical to that given in reference 18 except for the quantity B. The quantity B is a constant established from laboratory calibrations of the sonic throat. For the sonic throats used, a value of B of 0.95 was determined from laboratory tests.

Internal Drag

The internal drag D_I was evaluated as the change in momentum of the internal flow from free-stream conditions to station e aft of the exit where the static pressure is equal to free-stream static pressure. In order to provide a consistent basis for evaluating internal drag, for inlets which induct boundary layer, this same procedure is employed. The internal drag evaluated, however, includes the momentum losses in the boundary layer ahead of the duct entrance.

For evaluation of the internal drag, it was assumed that the flow at the exit was symmetrical about the horizontal center line of the duct. The exit area was divided into eight equal areas and the flow through each area was determined from the pitot-static measurements assigned to the area. The internal drag contributed by the flow through one of the eight areas was evaluated from the relationship

$$(D_I)_n = (m)_n \left[V_o - (V_e)_n \right] \tag{15}$$

where

$$(V_e)_n = (a_e)_n \, (M_e)_n \tag{16}$$

[redacted]

where the subscript n refers to one of the eight portions of the flow.

The quantity $(M_e)_n$ was determined by assuming no losses in total pressure from the exit to station e. Thus,

$$\frac{p_o}{(H_{134})_n} = \left[1 + \frac{\gamma-1}{2}(M_e)_n^2\right]^{-\frac{\gamma}{\gamma-1}} \tag{17}$$

The speed of sound at station e was evaluated (assuming the total temperature of the flow constant) by the relationship

$$\frac{(T_e)_n}{(T_o)_{total}} = \left[1 + 0.2(M_e)_n^2\right]^{-1} \tag{18}$$

Thus,

$$(a_e)_n = \sqrt{\gamma R (T_e)_n} \tag{19}$$

where R is the gas constant.

The internal drags were then summed over the area of one duct. The model internal drag was taken as double this value.

REFERENCES

1. Frick, Charles W., Davis, Wallace F., Randall, Lauros M., and Mossman, Emmet A.: An Experimental Investigation of NACA Submerged-Duct Entrances. NACA ACR 5I20, 1945.

2. Mossman, Emmet A., and Randall, Lauros M.: An Experimental Investigation of the Design Variables for NACA Submerged Entrances. NACA RM A7I30, 1948.

3. Mossman, Emmet A., and Gault, Donald E.: Development of NACA Submerged Inlets and a Comparison with Wing Leading-Edge Inlets for a 1/4-Scale Model of a Fighter Airplane. NACA RM A7A31, 1947.

4. Martin, Norman J.: Tests of Submerged Duct Installation on the Ryan FR-1 Airplane in the Ames 40- by 80-Foot Wind Tunnel. NACA RM A7D14, 1947.

5. Martin, Norman J.: Tests of Submerged Duct Installation on a Modified Fighter Airplane in the Ames 40- by 80-Foot Wind Tunnel. NACA RM A7I29, 1947.

6. Martin, Norman J., and Holzhauser, Curt A.: An Experimental Investigation at Large Scale of Several Configurations of an NACA Submerged Air Intake. NACA RM A8F21, 1948.

7. Delany, Noel K.: An Investigation of Submerged Air Inlets on a 1/4-Scale Model of a Typical Fighter-Type Airplane. NACA RM A8A20, 1948.

8. Hall, Charles F., and Barclay, F. Dorn: An Experimental Investigation of NACA Submerged Inlets at High Subsonic Speeds. I - Inlets Forward of the Wing Leading Edge. NACA RM A8B16, 1948.

9. Hall, Charles F., and Frank, Joseph L.: Ram-Recovery Characteristics of NACA Submerged Inlets at High Subsonic Speeds. NACA RM A8I29, 1948.

10. Martin, Norman J., and Holzhauser, Curt A.: An Experimental Investigation at Large Scale of Single and Twin NACA Submerged Side Intakes at Several Angles of Sideslip. NACA RM A9F20, 1949.

11. Mossman, Emmet A.: A Comparison of Two Submerged Inlets at Subsonic and Transonic Speeds. NACA RM A9F16, 1949.

[redacted]

12. Axelson, John A., and Taylor, Robert A.: Preliminary Investigation of the Transonic Characteristics of an NACA Submerged Inlet. NACA RM A50C13, 1950.

13. Rolls, L. Stewart, and Rathert, George A., Jr.: Tests of a Small-Scale NACA Submerged Inlet at Transonic Mach Numbers. NACA RM A9L29, 1950.

14. Baals, Donald D., Smith, Norman F., and Wright, John B.: The Development and Application of High-Critical-Speed Nose Inlets. NACA Rep. 920, 1948.

15. Sears, R. I., and Merlet, C. F.: Flight Determination of the Drag and Pressure Recovery of an NACA 1-40-250 Nose Inlet at Mach Numbers from 0.9 to 1.8. NACA RM L50L18, 1951.

16. Mills, W. H.: Calculation of Trajectory and Drag Function from Accelerometer Data. Aberdeen Proving Ground, Maryland. Ballistic Res. Lab. Rep. No. 443, 1943.

17. Lindsey, W. F.: Calibration of Three Temperature Probes and a Pressure Probe at High Speeds. NACA ARR, April, 1942.

18. Davis, Wallace F., Brajnikoff, George B., Goldstein, David L., and Spiegel, Joseph M.: An Experimental Investigation at Supersonic Speeds of Annular Duct Inlets Situated in a Region of Appreciable Boundary Layer. NACA RM A7G15, 1947.

[redacted]

TABLE I.- MODEL INSTRUMENTS

Item	Function	Range	Estimated accuracy
NACA recording accelerometer	To measure $\frac{D_T}{W}$	0 to 0.5 $\frac{D_T}{W}$	$\pm 0.0025 \frac{D_T}{W}$
NACA three-mirror airspeed and altitude recorder	To measure indicated impact pressure $H_o - p_i$	0 to 21 in. Hg	±0.04 in. Hg
Manometer cells	4 cells to measure $(H)_{86.5} - H_o$	0 to −10 in. Hg	±0.06 in. Hg
	4 cells to measure $(H)_{134} - H_o$	0 to −15 in. Hg	±0.09 in. Hg
	4 cells to measure $(p)_{134} - p_i$	+3 to −3 in. Hg	±0.04 in. Hg
	8 cells for other measurements (pressure distribution) (sonic throat pressures) (pressures at inlet on nose-inlet model)	----	----
NACA instrument timer	To actuate common timing circuit	1/2 sec. or 1/10 sec. timing intervals	±1 sec. in 1200 sec.

TABLE II.- AIRPLANE INSTRUMENTS

Item	Function	Range	Estimated accuracy
NACA three-mirror airspeed recorder	To measure airplane impact pressure H_o-p_o	0 to 5.4 in. Hg	±0.01 in. Hg
NACA three-mirror altitude recorder	To measure p_o	3.5 to 11 in. Hg	±0.013 in. Hg
NACA three-mirror altitude recorder	To measure p_o	11 to 30 in. Hg	±0.029 in. Hg
NACA galvanometer and resistance bulb thermometer	To measure indicated free-stream temperature	-60° F to +70° F	±0.7° F
NACA sensitive altitude recorder	To check level flight conditions prior to release	5.2 to 6 in. Hg	±0.008 in. Hg
NACA instrument timer	To actuate common timing circuit	1/2 sec. intervals	± 1 sec. in 1200 sec.

[redacted]

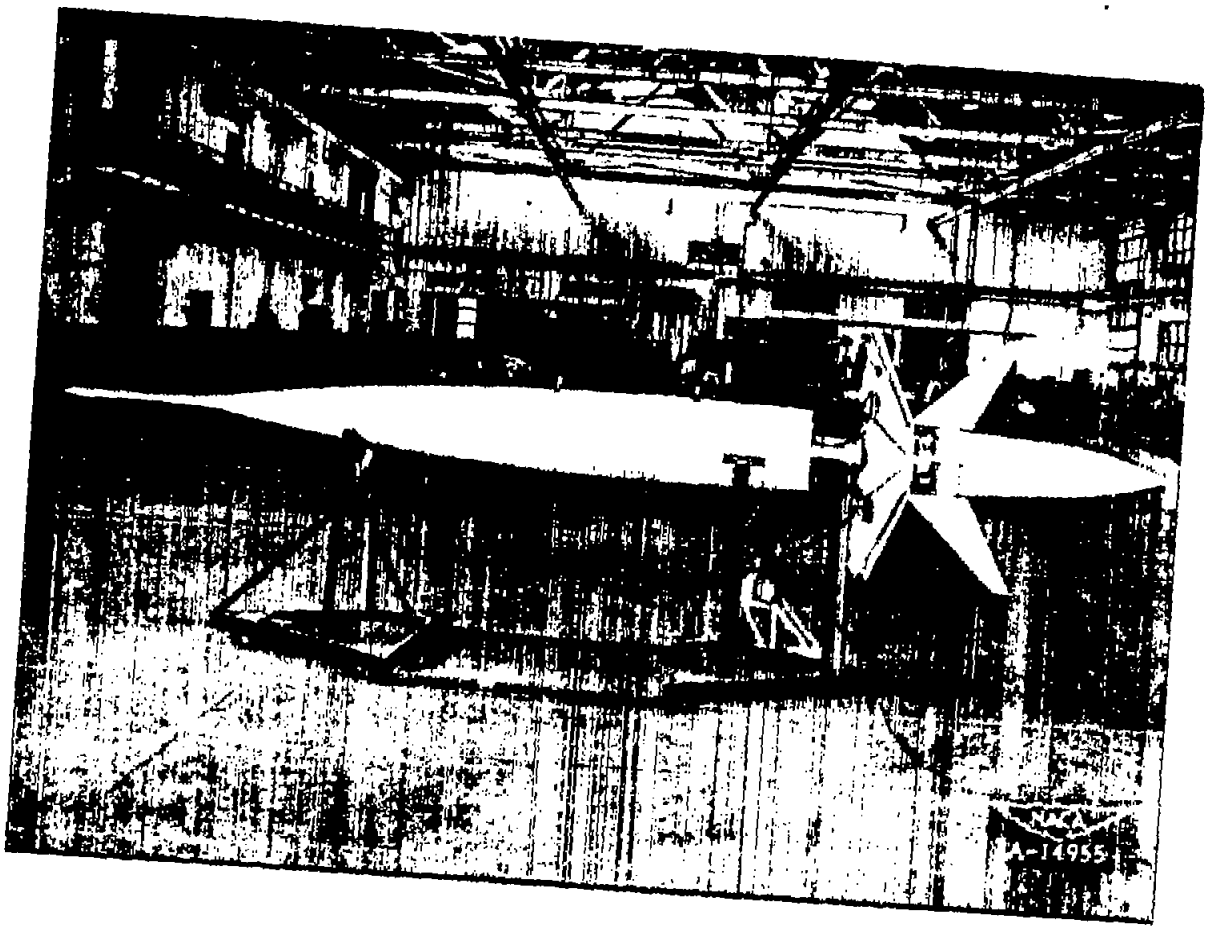

Figure 1.- Basic model with recovery brake extended.

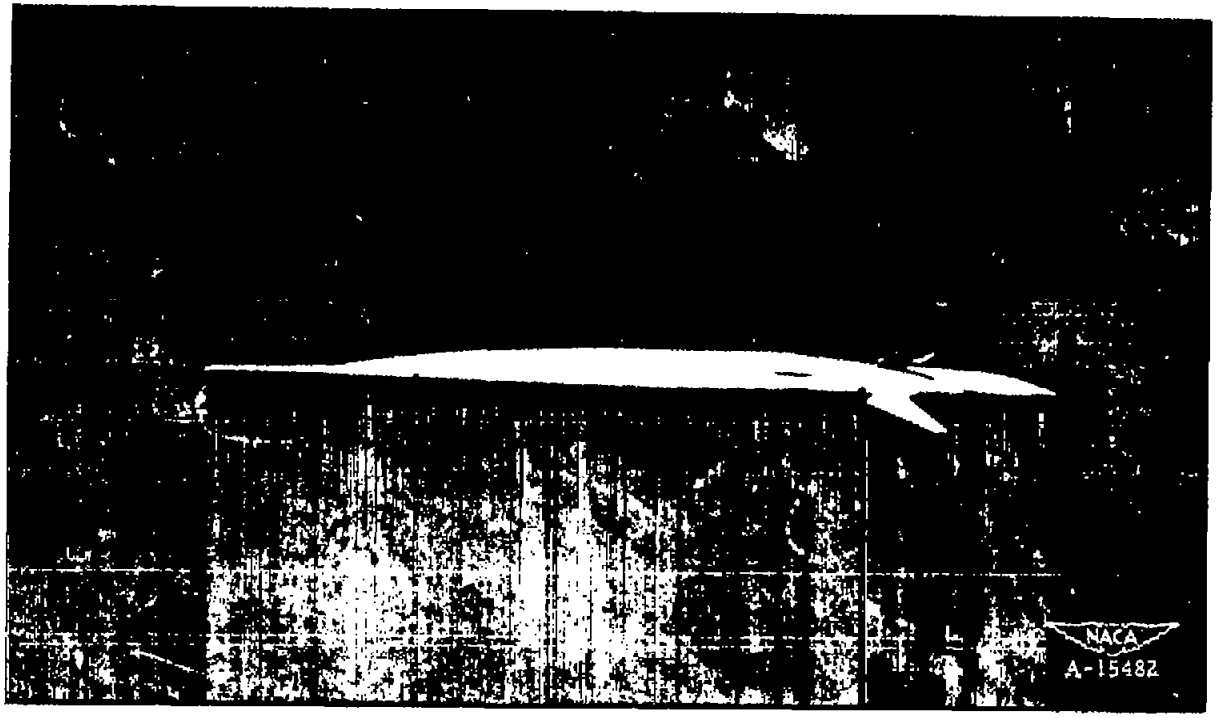

Figure 2.- Basic model after release from carrier airplane.

Figure 3.- Basic model after impact.

Table of Ordinates		
Station, inches	Outside radius, inches	
	R_1	R_2
0	1.19	- -
5.00	1.70	- -
10.00	2.43	- -
15.00	3.21	- -
20.00	3.90	- -
30.00	5.07	- -
40.00	6.02	- -
50.00	6.78	- -
60.00	7.39	- -
70.00	7.87	- -
80.00	8.20	- -
90.00	8.41	- -
100.00	8.49	- -
102.00	8.50	8.50
110.00	8.46	8.50
120.00	8.30	8.50
130.00	8.02	8.50
135.75	7.79	8.50
146.63	7.25	7.55
150.00	7.07	7.25
154.88	6.82	6.82
160.00	6.56	- -
170.00	6.07	- -
180.00	5.59	- -
192.63	4.89	- -
201.63	3.20	- -
211.00	0	- -

Specifications
Horizontal-tail area (incl 1.30ft² of fus.) 3.45 ft²
Vertical-tail area (incl 1.30ft² of fus.) 3.45 ft²
Model weight, 1057 lb
Center of gravity sta. 86.25
External wetted area (excluding fins) 8515 in.²

Note
All dimensions are in inches

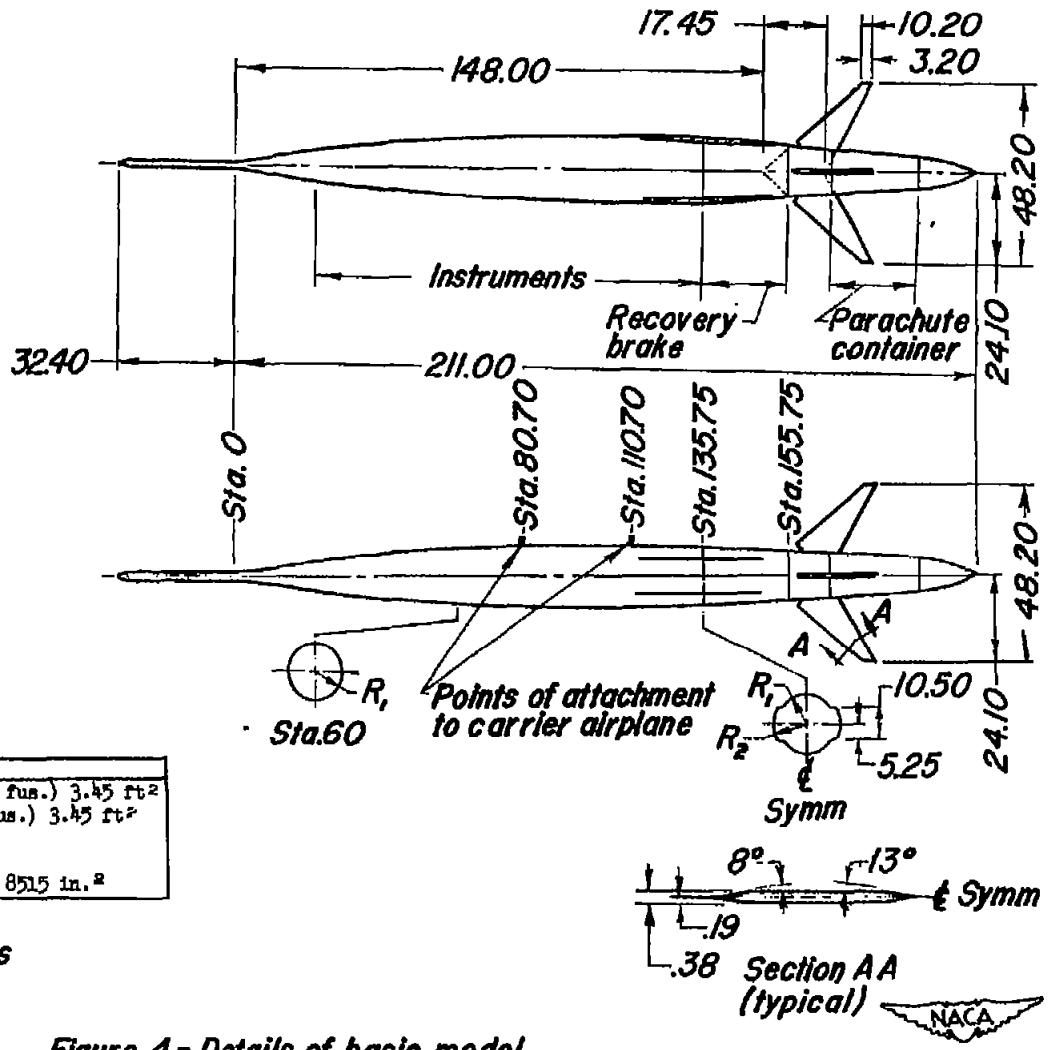

Figure 4.- Details of basic model.

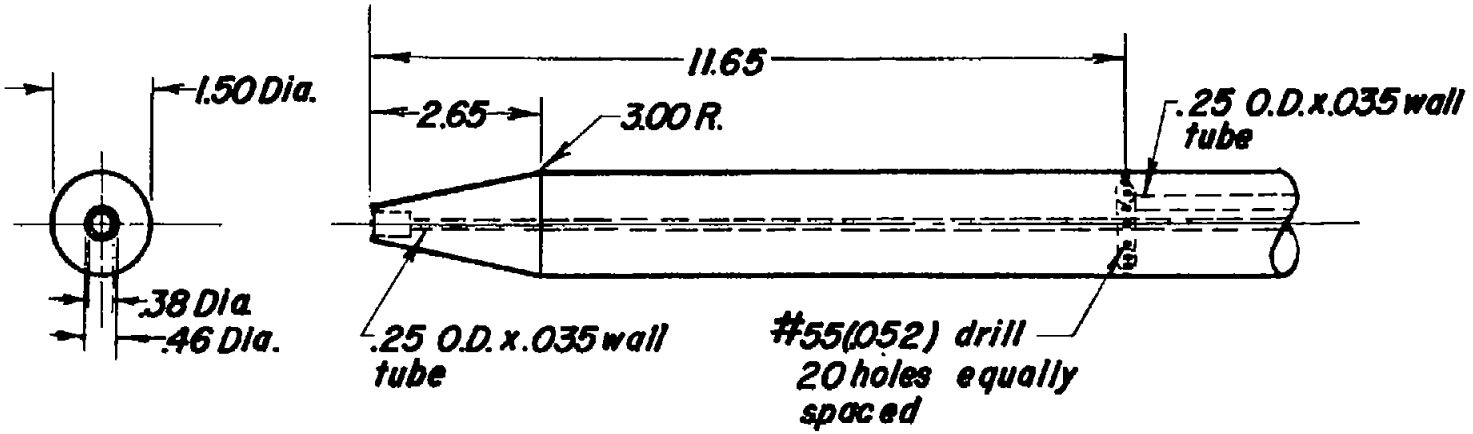

Figure 5.- Airspeed head.

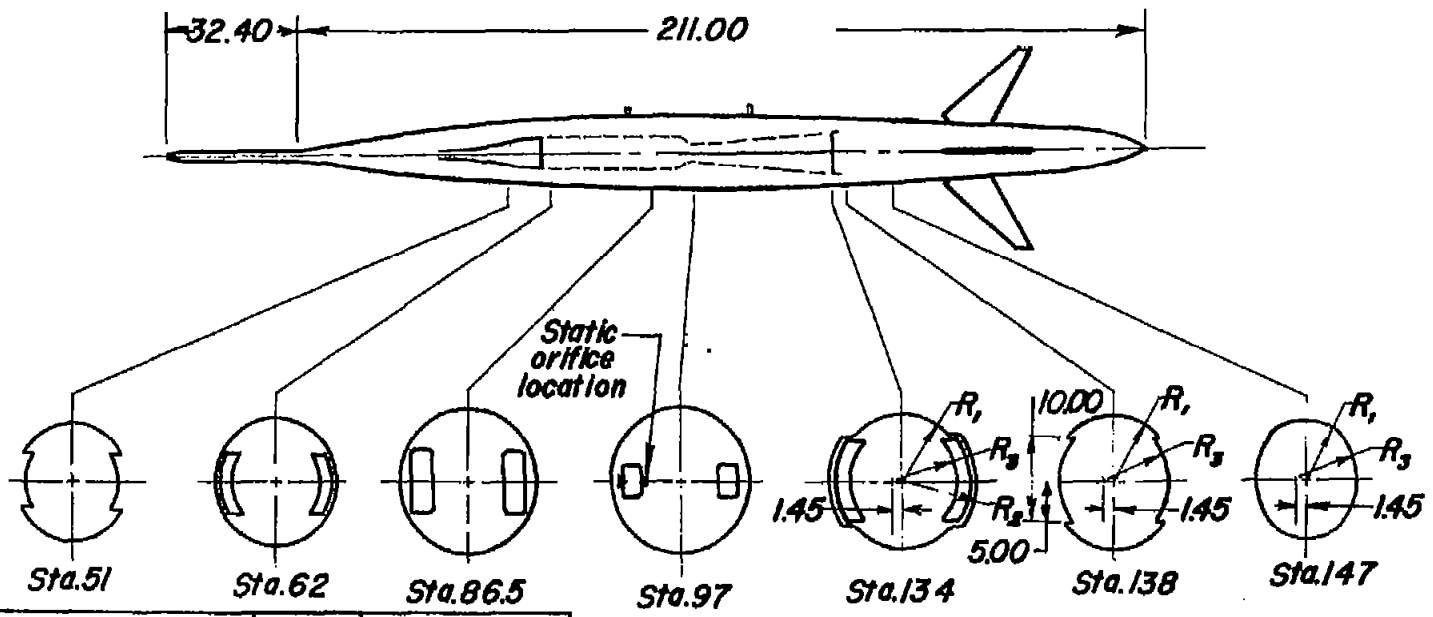

Areas (per duct)
Entrance 13.62 in.^{2} (sta.62)
16.89 in.^{2} (sta.86.5)
Entrance to throat 17.34 in.^{2} (sta.90)
Throats 1. 6.49 in.^{2}, 50-percent throat (sta.97)
2. 10.89 in.^{2}, 80-percent throat (sta.97)
Outlet 13.75 in.^{2}(sta.135.75)

Specifications
Center of gravity, sta.94.50
Model weight, 1121 lb.
External wetted area (excluding fins) 8,575 in.^{2}

Note

1. All dimensions are in inches
2. For ordinates see figure 4

Exit Dimensions			
Sta.	R_1	R_2	R_3
134.00	7.79	8.50	8.22
138.00	7.68	- -	8.22
147.00	7.21	- -	8.22

(a) Complete model.

Figure 6.– Details of submerged inlet model.

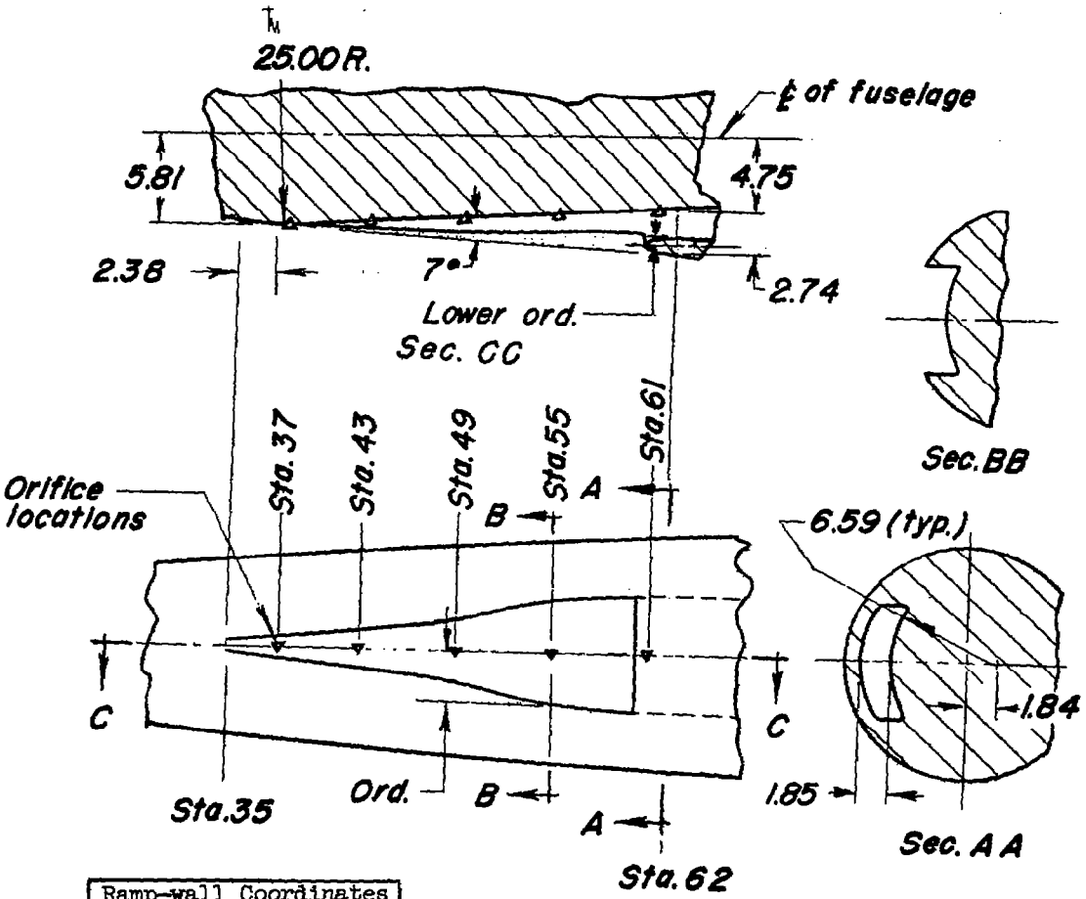

Ramp-wall Coordinates	
Sta.	Ordinates
35.00	0.31
37.50	.59
40.00	.87
42.50	1.16
45.00	1.44
47.50	1.72
50.00	2.27
52.50	2.82
55.00	3.37
57.50	3.67
60.00	3.69
62.00	3.69

Lip Ordinates		
Sta.	Upper ord.	Lower ord.
60.00	0	0
60.25	.22	.23
60.50	.31	.30
60.75	.37	.35
61.00	.42	.38
61.38	.48	.40
62.00	.51	.39
L.E. radius = 0.17		

Note
All dimensions are in inches

(b) Submerged inlet.
Figure 6.- Continued.

[redacted]

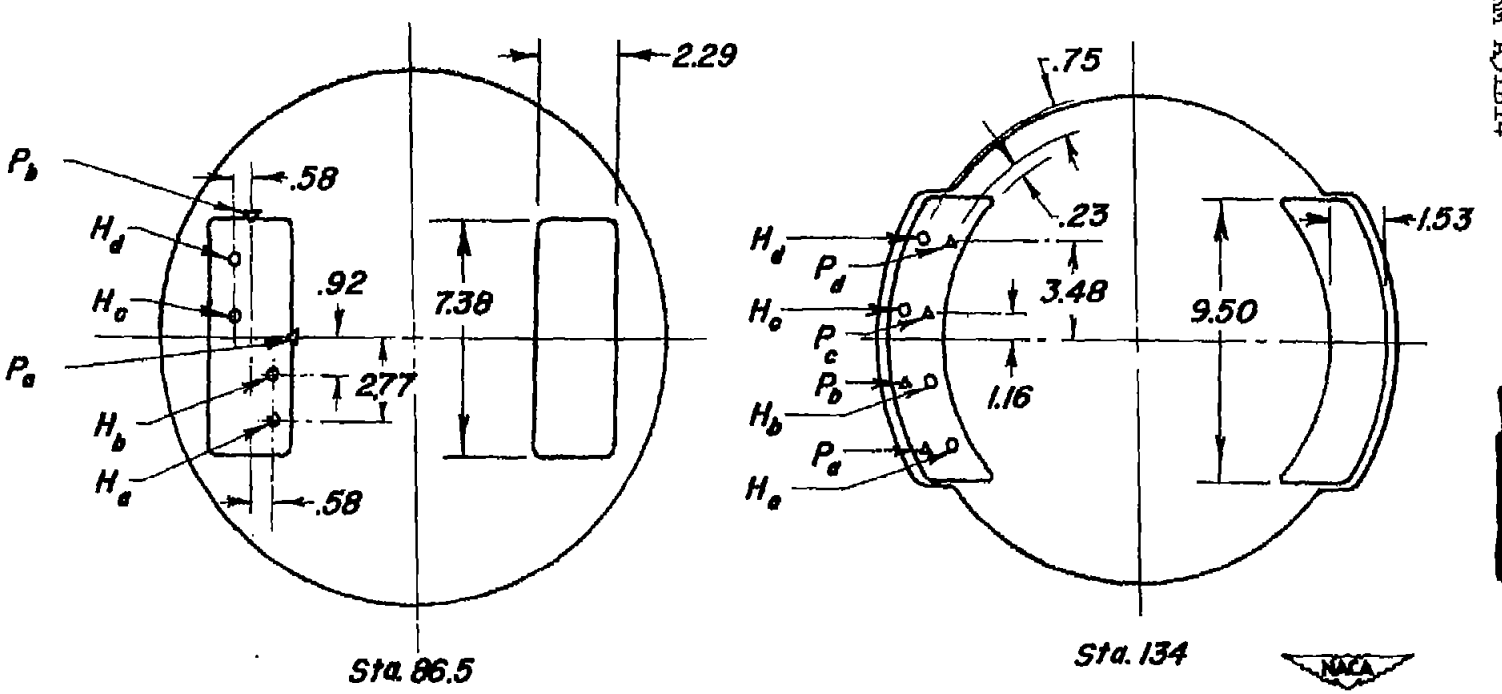

Note
1. H-Total pressure
2. P-Static pressure
3. All dimensions are in inches

(c) Location of pressure probes and orifices at stations 86.5 and 134.
Figure 6.- Concluded.

Figure 7.- Submerged-inlet model.

Table of Ordinates		
Sta.	R_1	R_2
0	3.17	3.17
.20	3.43	3.04
.41	3.53	3.04
.61	3.61	3.04
.82	3.67	3.04
1.53	3.85	3.04
2.55	4.06	3.04
5.00	4.46	3.06
8.16	4.87	3.31
10.20	5.10	3.49
14.28	5.50	3.88
20.40	5.98	4.66
24.48	6.26	5.18
27.00	6.42	5.48
30.00	6.60	- -
40.80	7.16	- -
49.98	7.54	- -
61.20	7.92	- -
70.00	8.15	- -
79.56	8.33	- -
91.80	8.47	- -
102.00	8.50	- -

Areas (Per duct)	
Entrance	13.62 in.^{2} (sta.0)
	14.74 in.^{2} (sta.30)
Entrance to throat	17.34 in.^{2} (sta.90)
Throats	1. 6.49 in.^{2}, 50-percent throat (sta.97)
	2. 10.89 in.^{2}, 80-percent throat (sta.97)
Outlet	13.75 in.^{2} (sta.135.75)

Specifications	
Model weight, 1059 lb	
Center of gravity, sta. 91.00	
External wetted area (excluding fins)	9,124. in.^{2}

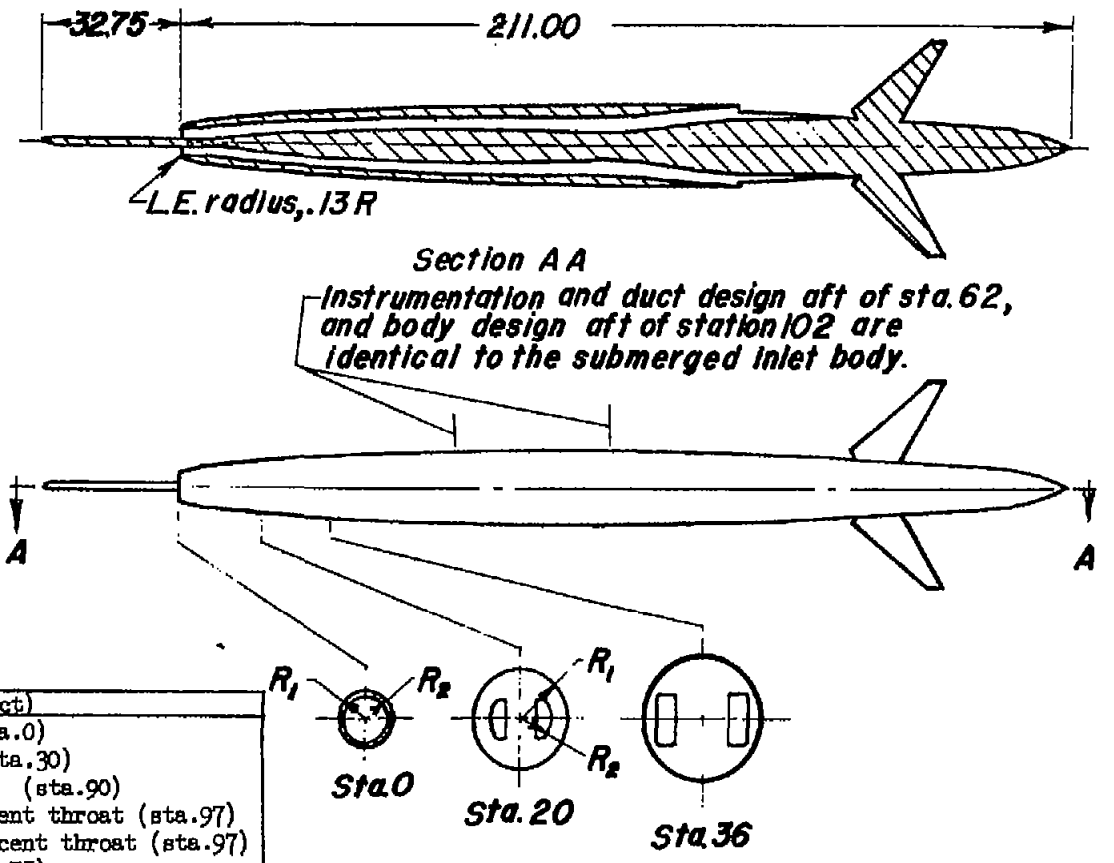

(a) Complete model.

Figure 8.- Details of NACA series I nose inlet model.

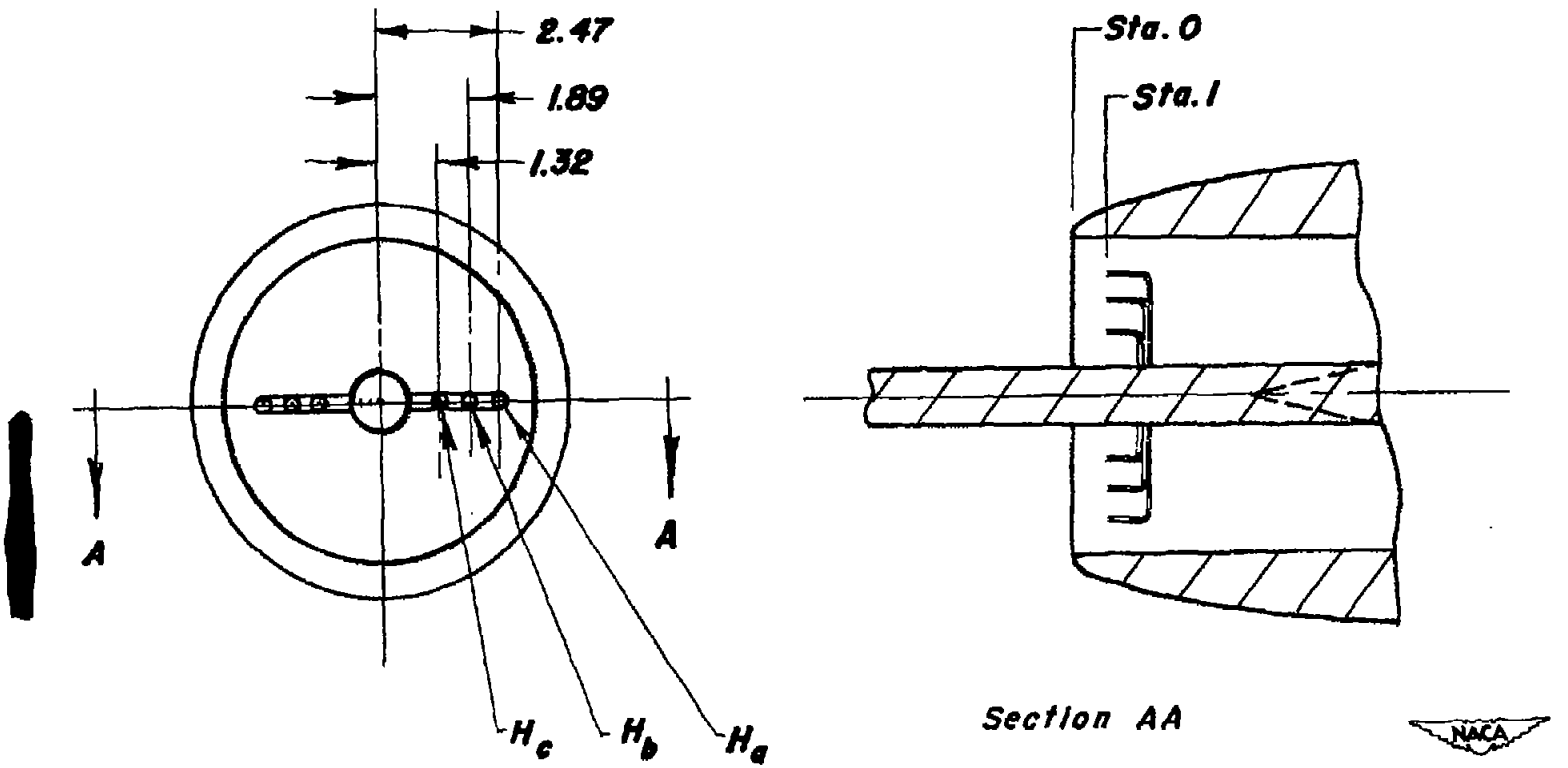

Note
All dimensions are in inches

(b) Pressure probes at station 1.

Figure 8.- Concluded.

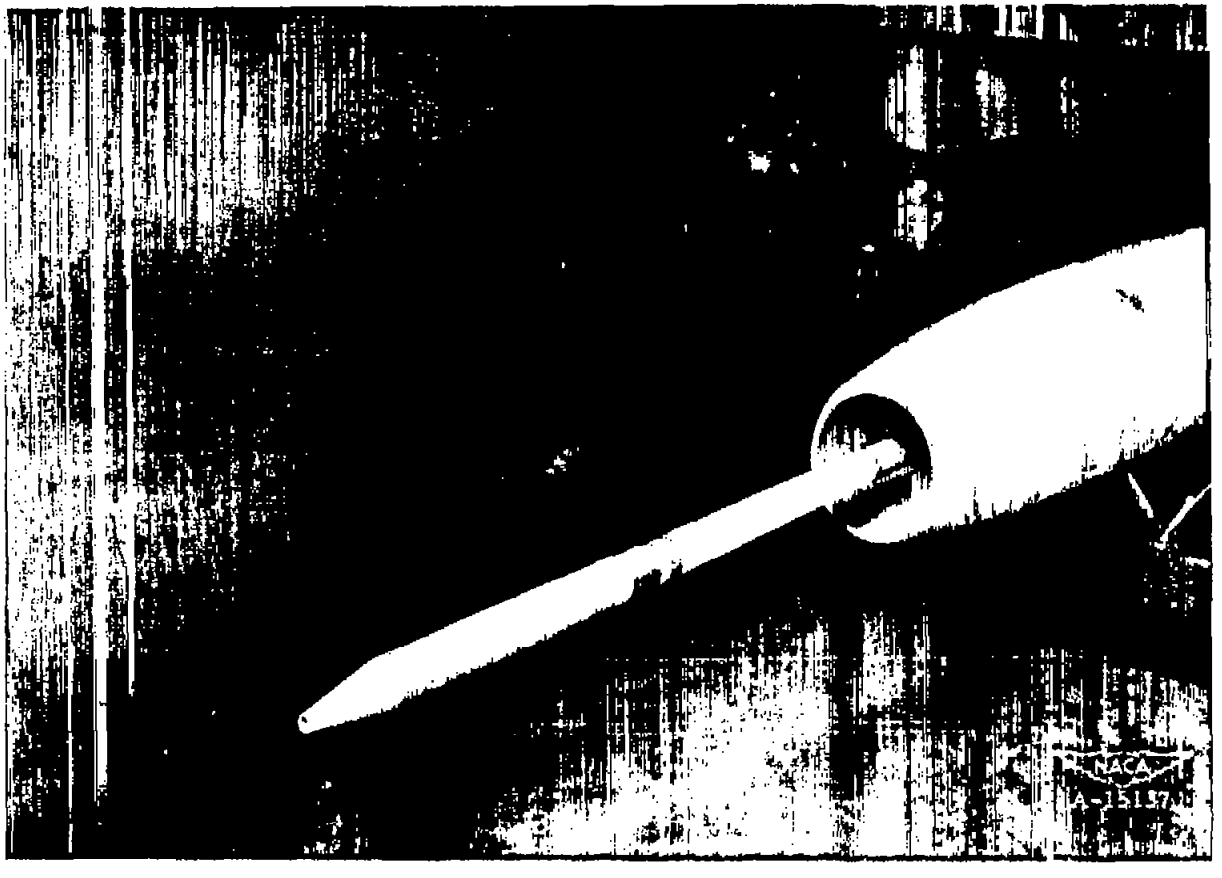

Figure 9.- Detail photograph of nose inlet.

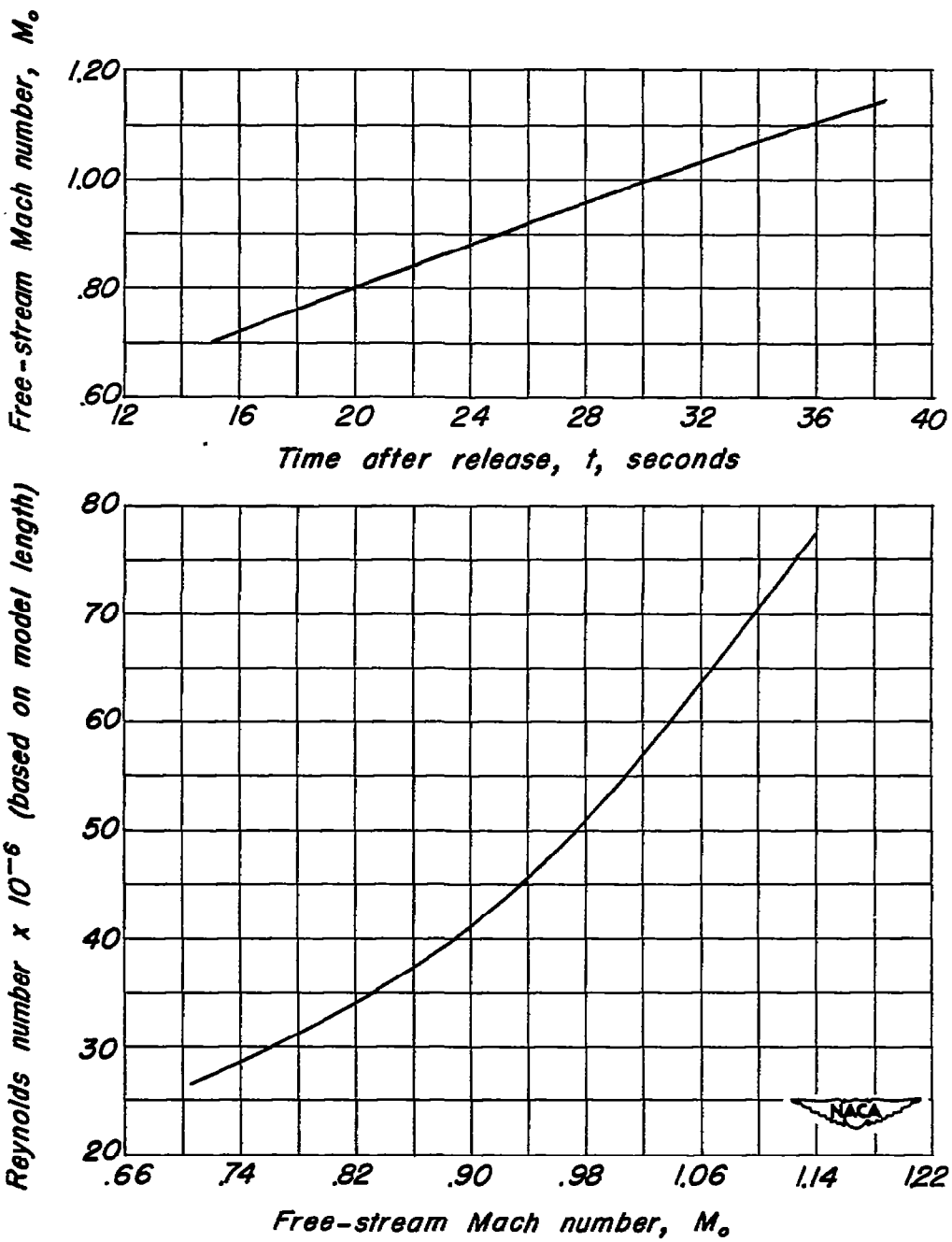

Figure 10.- Typical variation of Mach number with time and Reynolds number with Mach number during free fall of model.

[redacted]

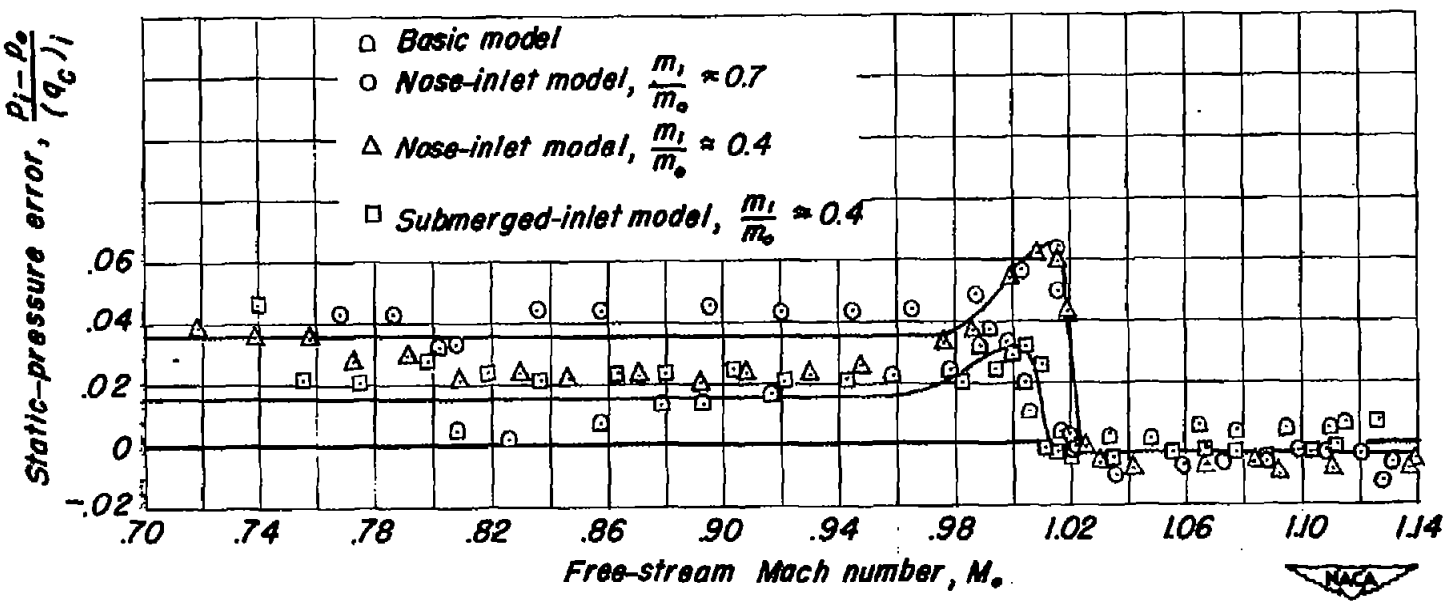

Figure 11.- Variation of airspeed head static-pressure error with Mach number.

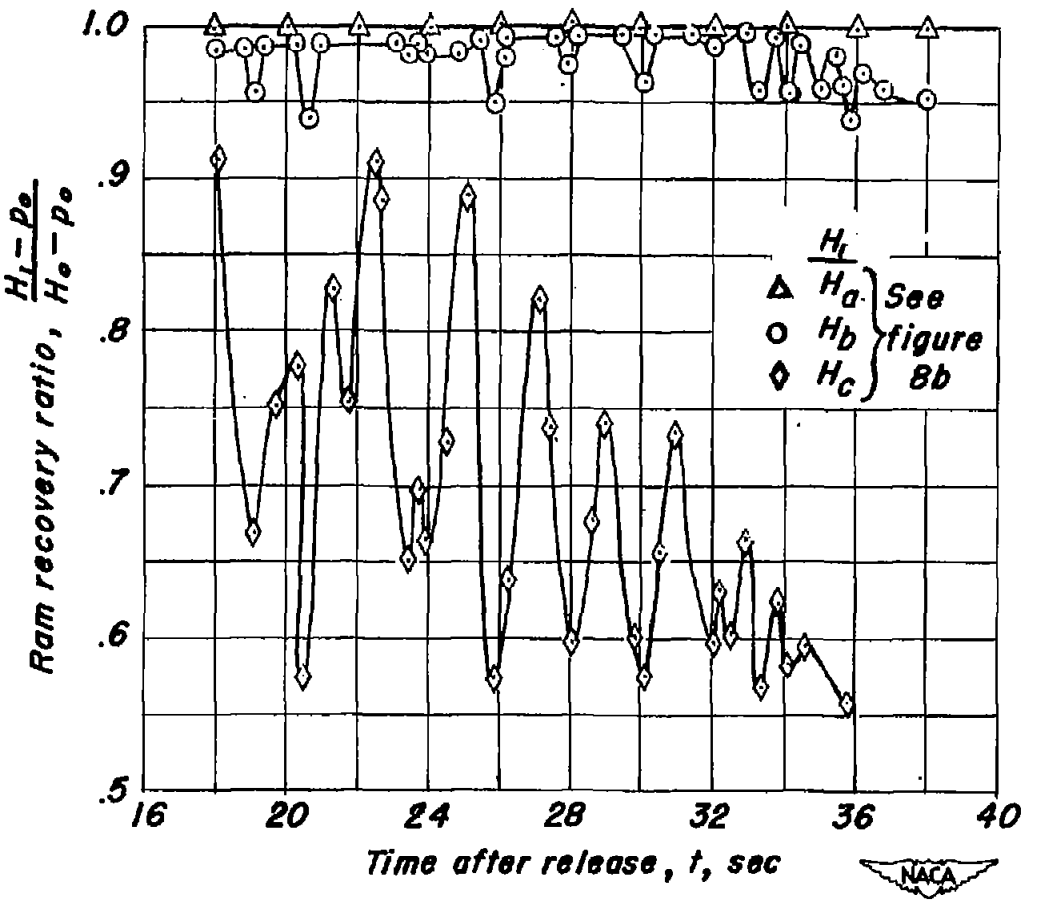

Figure 12.– Pressure recovery measurements at entrance of nose inlet, $\frac{m_1}{m_o} \approx 0.7$

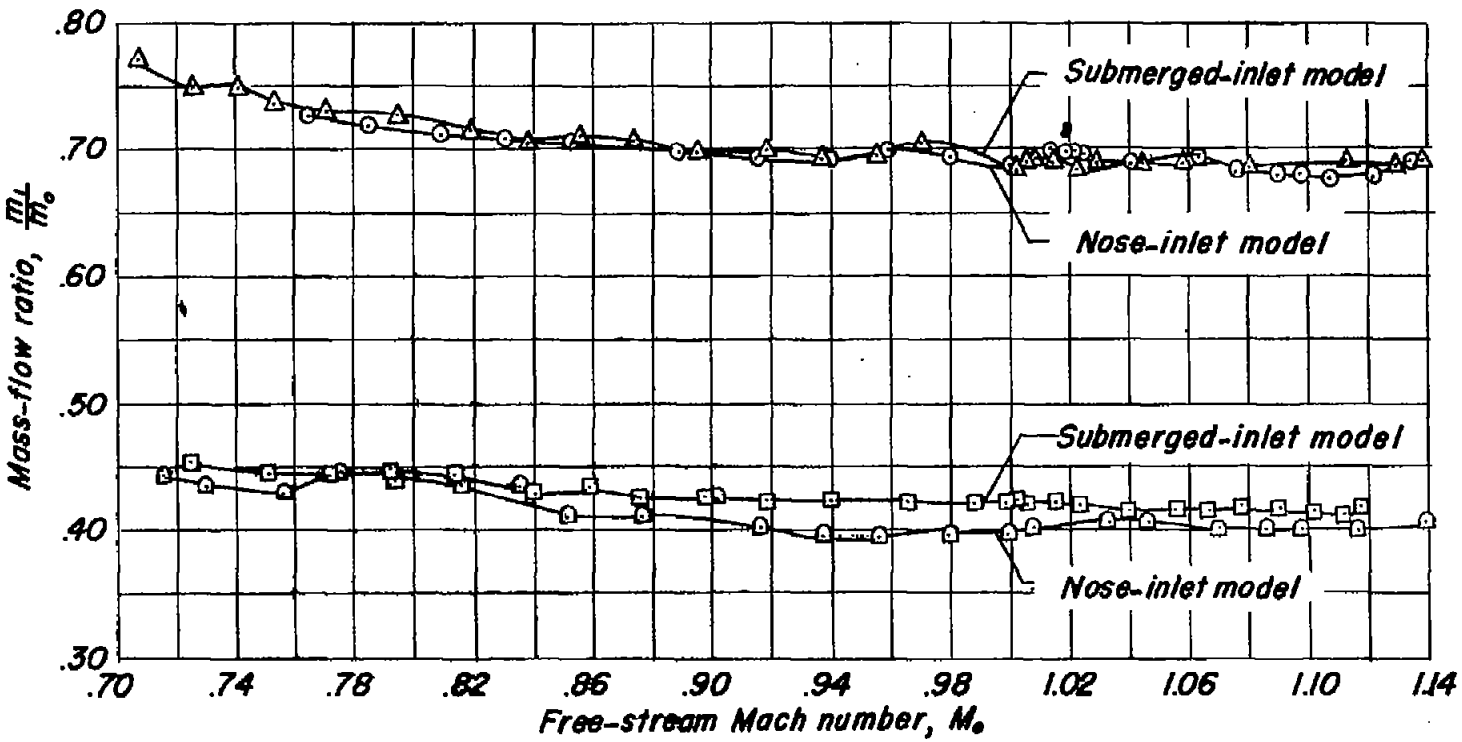

Figure 13.- Variation of mass-flow ratio with Mach number for submerged- and nose-inlet models.

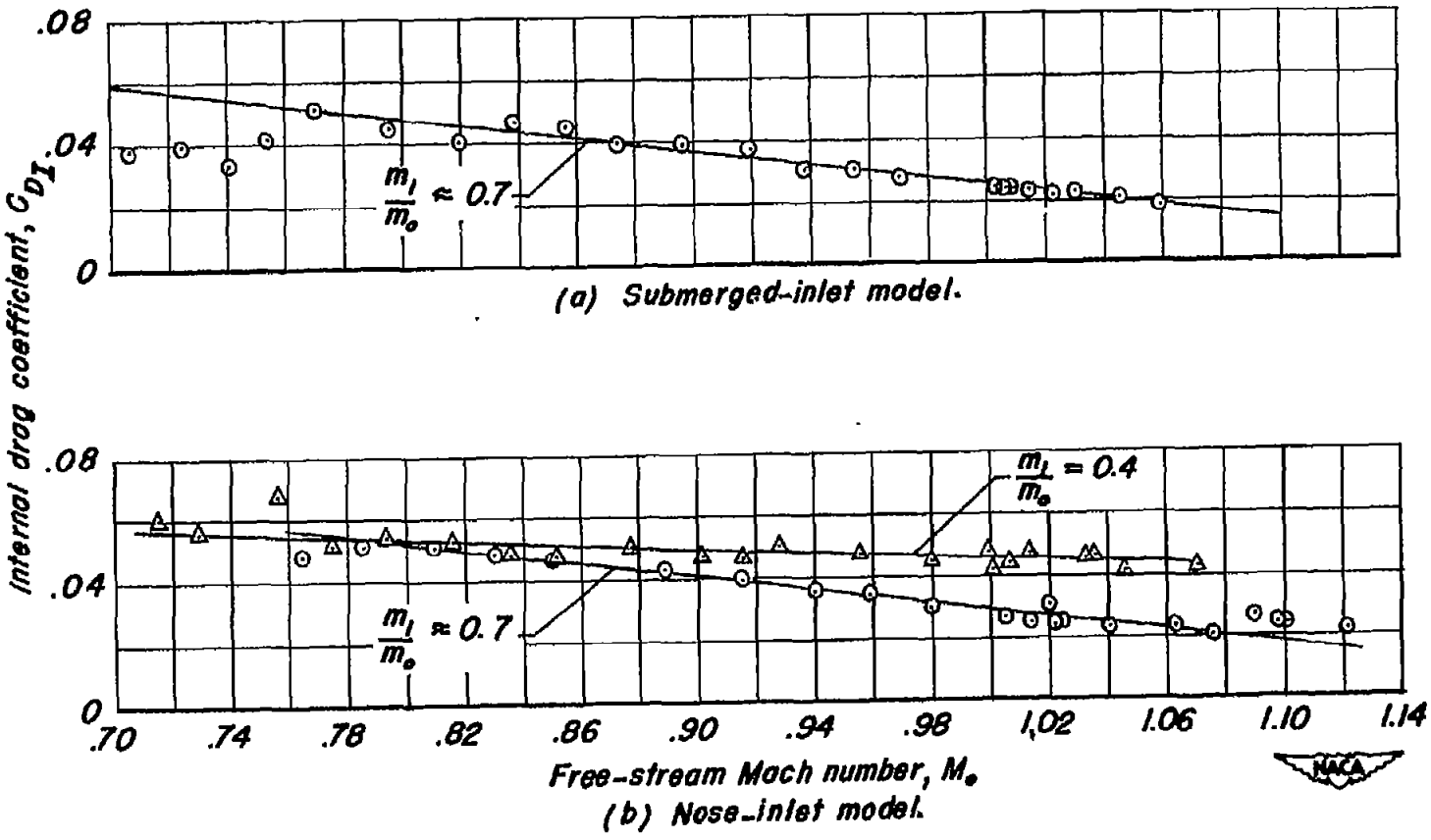

Figure 14.–Variation of internal drag coefficient with Mach number for submerged- and nose-inlet models.

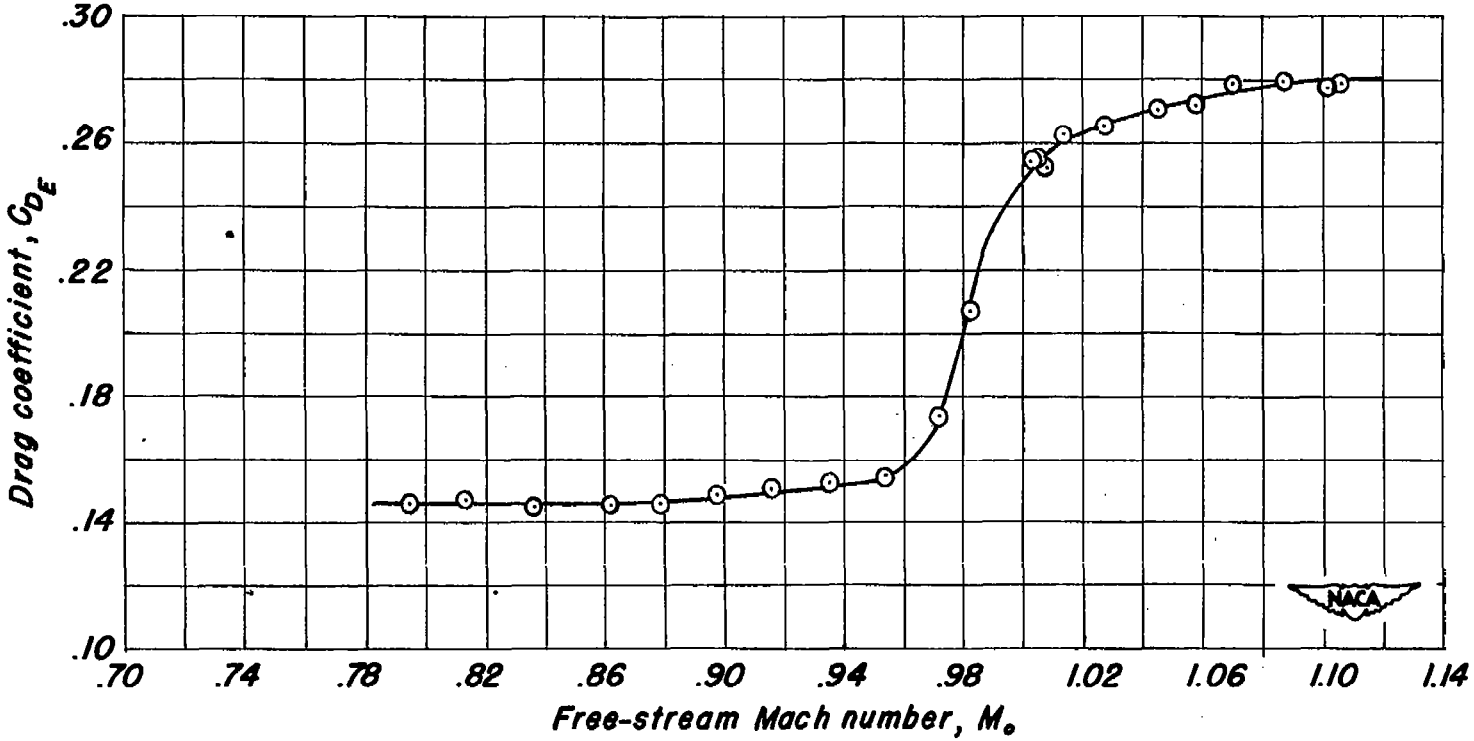

Figure 15.- Variation of drag coefficient of basic model with Mach number.

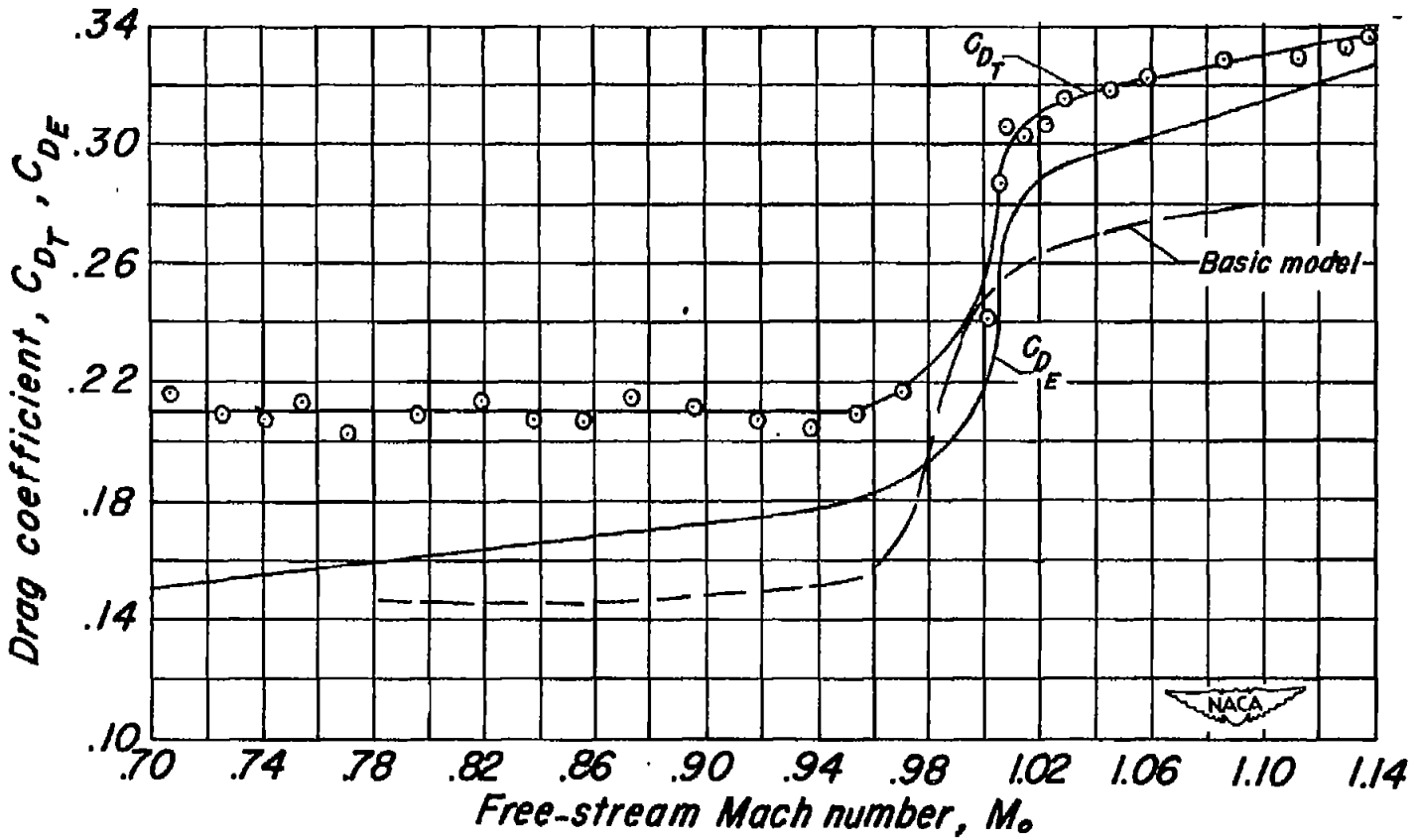

Figure 16.–Variation of total and external drag coefficients of submerged-inlet model with Mach number at a mass flow ratio of 0.7.

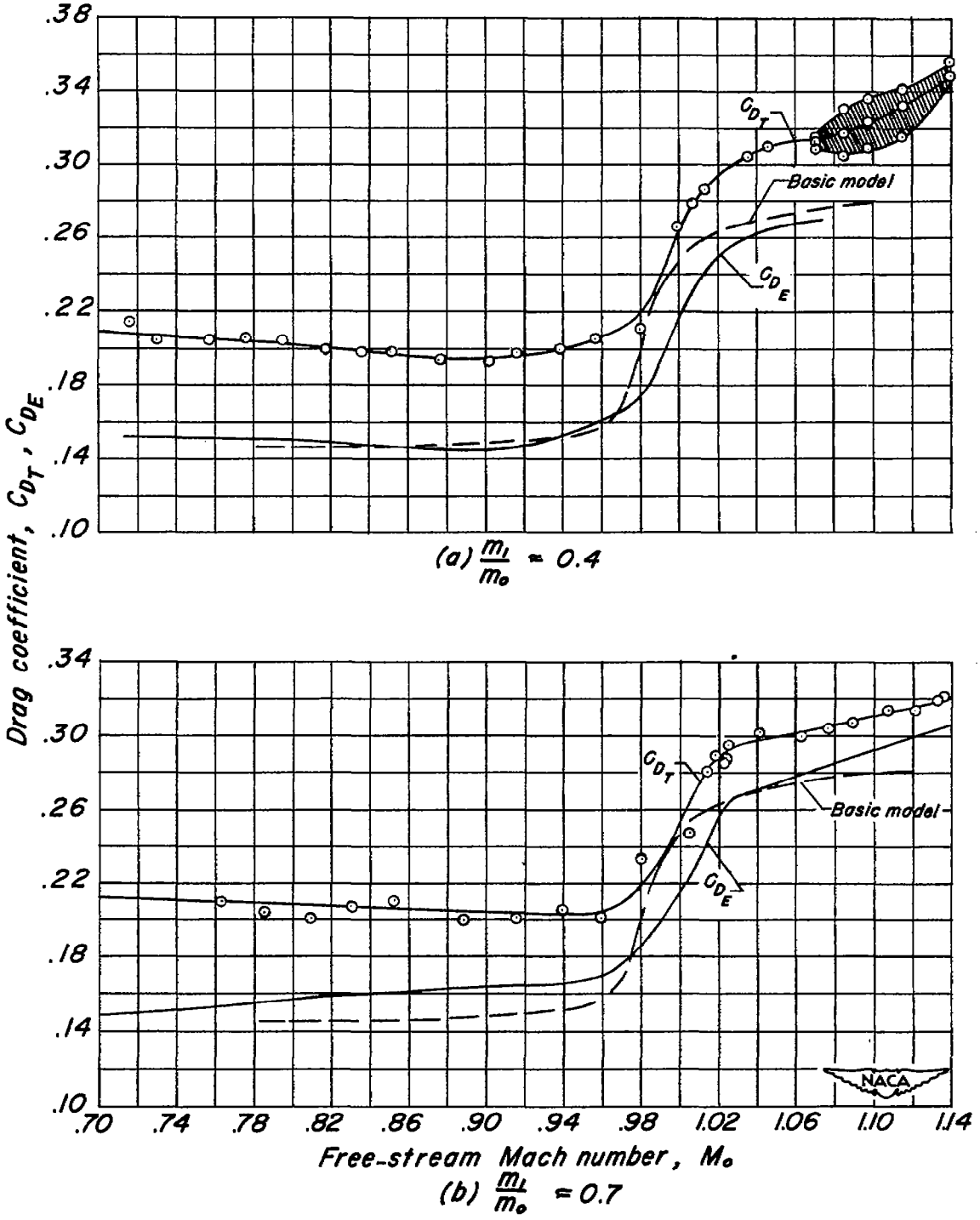

Figure 17.-Variation of total and external drag coefficients of nose-inlet model with Mach number.

[redacted]

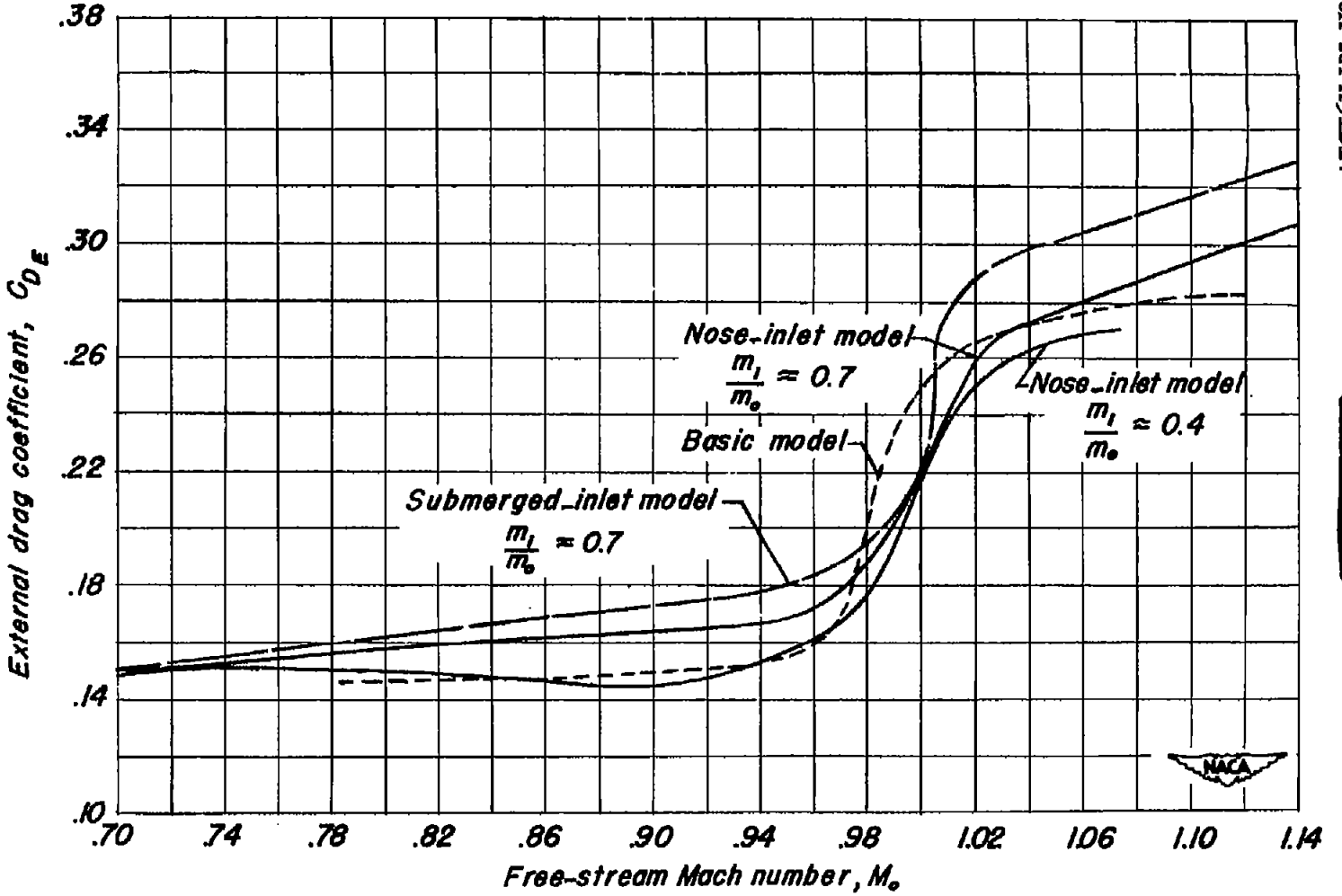

Figure 18.- Variation of external drag coefficients of models with Mach number.

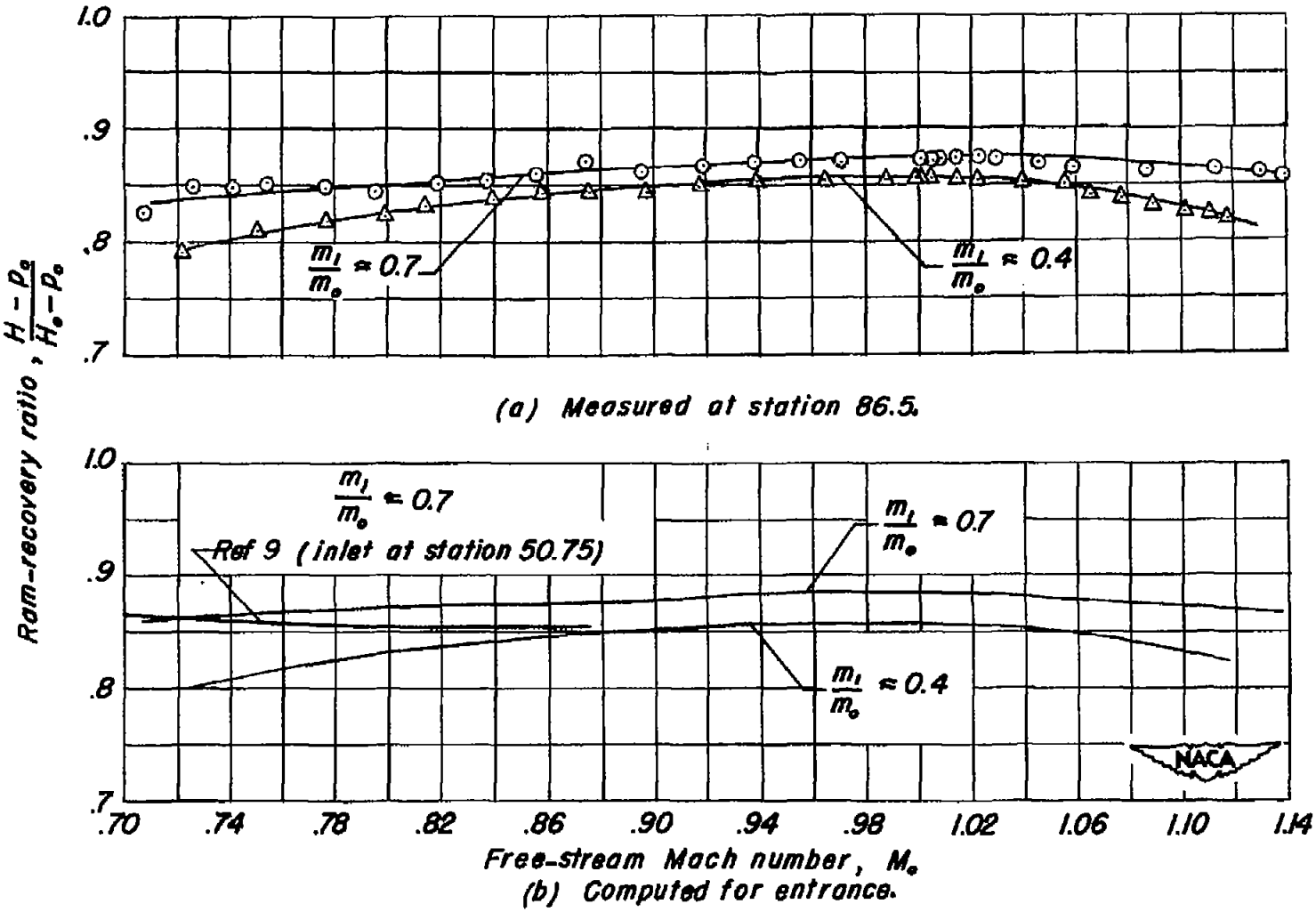

Figure 19.- Variation of ram-recovery ratio with Mach number for submerged-inlet model.

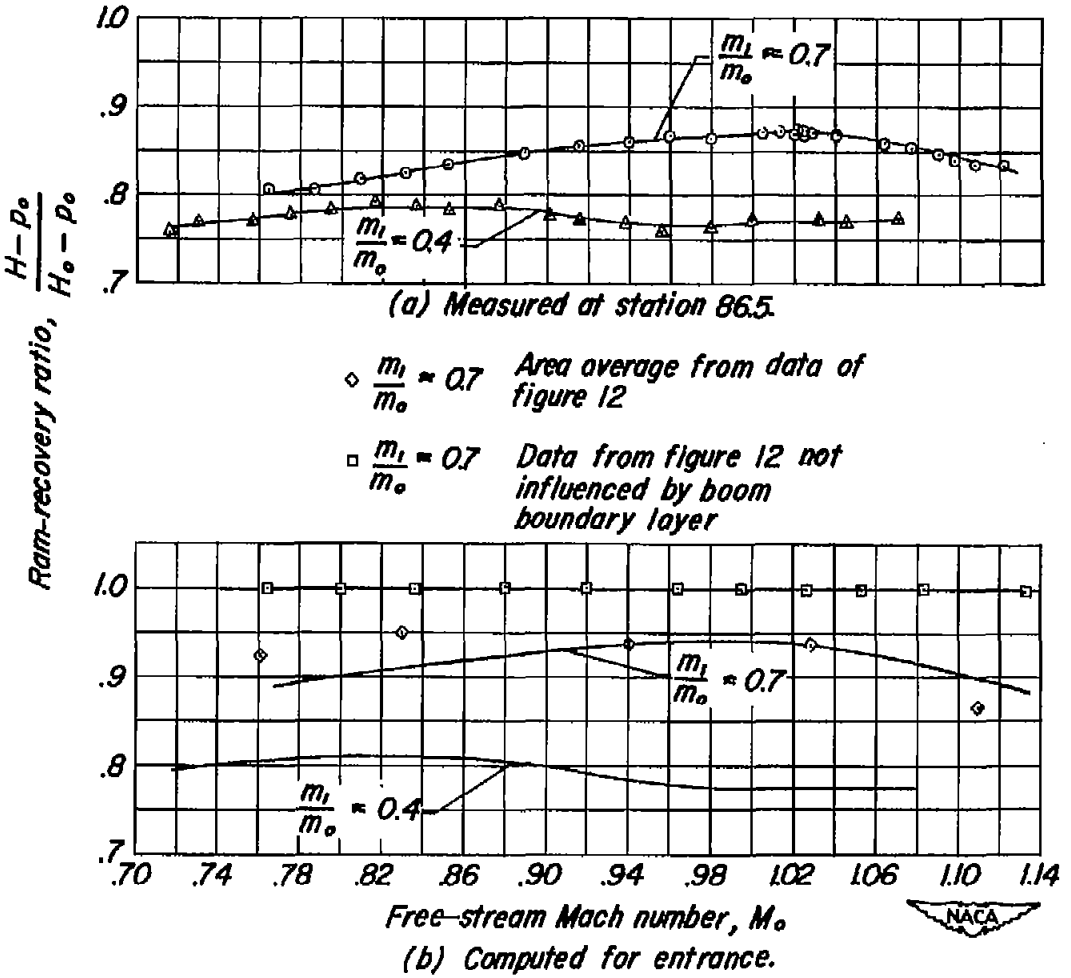

Figure 20.-Variation of ram-recovery ratio with Mach number for nose-inlet model.

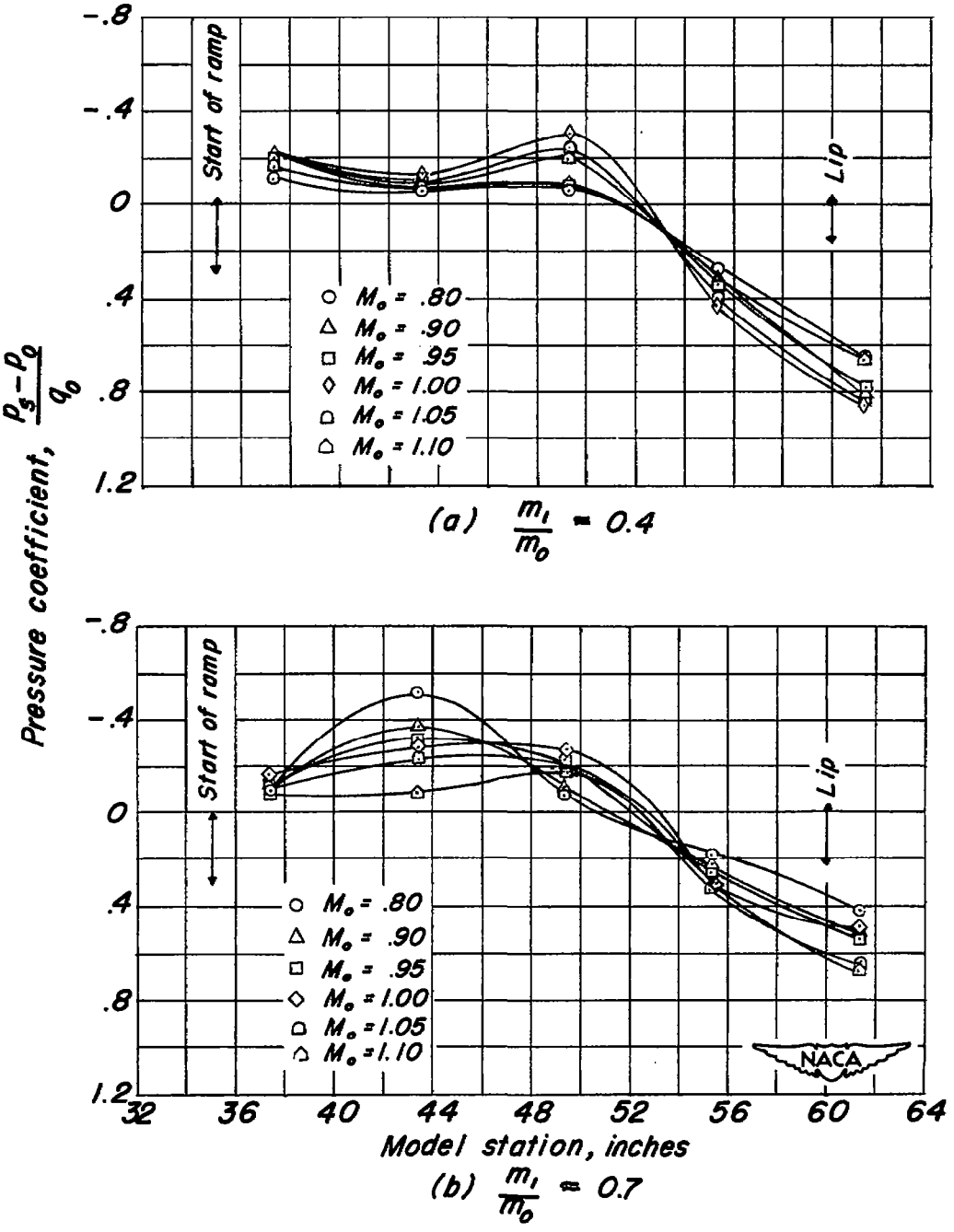

Figure 21.- Pressure distribution along ramp of submerged inlet at various Mach numbers.

[redacted]

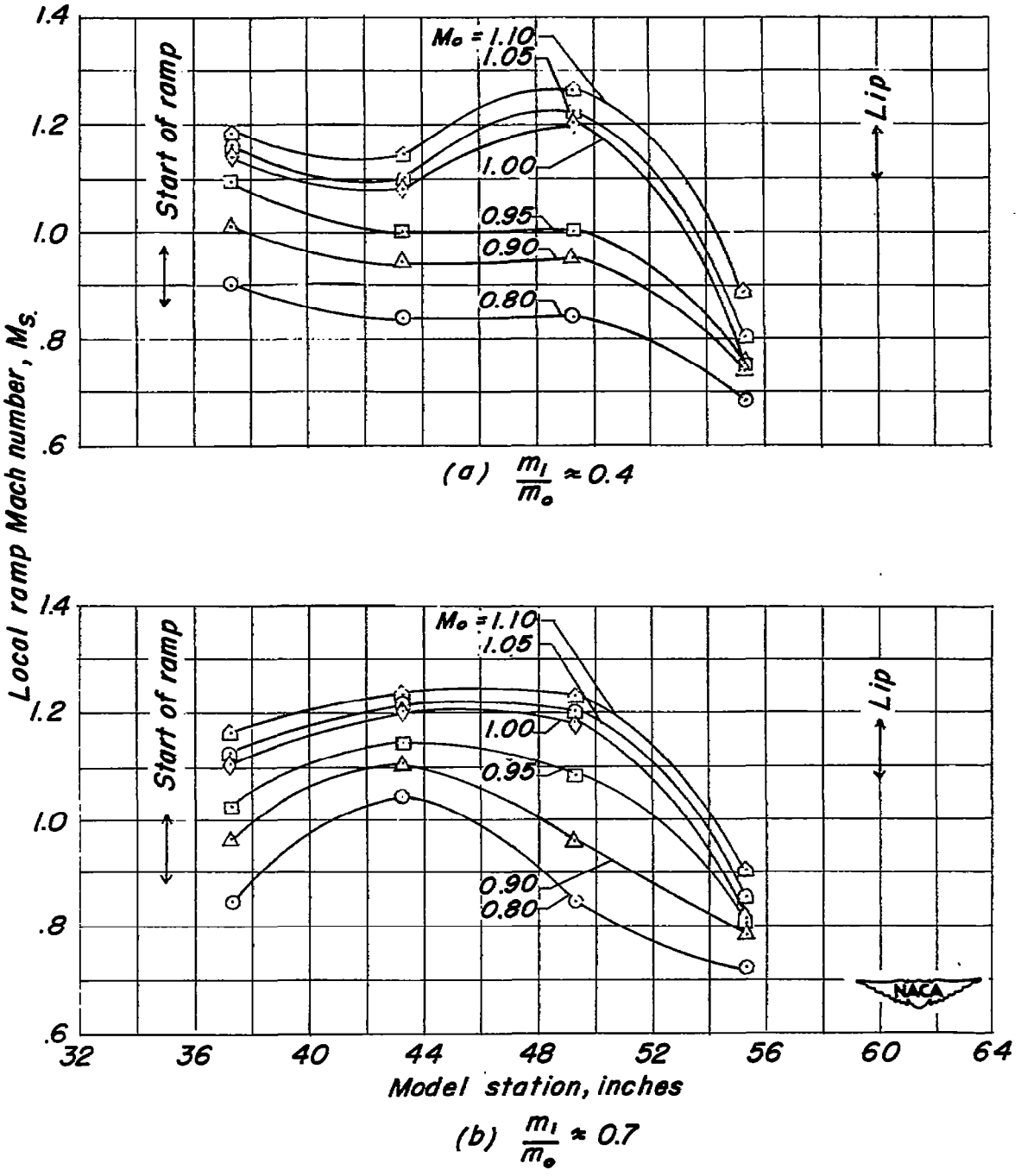

Figure 22.- Mach number distribution along ramp of submerged inlet at various Mach numbers.

[redacted]